NASA/TM–2018-219804

A Study of Shape Memory Polymer Based Slat-Cove Filler

Jin Ho Kang
National Institute of Aerospace, Hampton, Virginia

Emilie J. Siochi and Travis L. Turner
Langley Research Center, Hampton, Virginia

Ronald K. Penner and Richard Thomas
Science & Technology Corporation, Hampton, Virginia

Sean Brown
Oregon State University, Corvallis, Oregon

July 2018

NASA STI Program . . . in Profile

Since its founding, NASA has been dedicated to the advancement of aeronautics and space science. The NASA scientific and technical information (STI) program plays a key part in helping NASA maintain this important role.

The NASA STI program operates under the auspices of the Agency Chief Information Officer. It collects, organizes, provides for archiving, and disseminates NASA's STI. The NASA STI program provides access to the NTRS Registered and its public interface, the NASA Technical Reports Server, thus providing one of the largest collections of aeronautical and space science STI in the world. Results are published in both non-NASA channels and by NASA in the NASA STI Report Series, which includes the following report types:

- TECHNICAL PUBLICATION. Reports of completed research or a major significant phase of research that present the results of NASA Programs and include extensive data or theoretical analysis. Includes compilations of significant scientific and technical data and information deemed to be of continuing reference value. NASA counter-part of peer-reviewed formal professional papers but has less stringent limitations on manuscript length and extent of graphic presentations.

- TECHNICAL MEMORANDUM. Scientific and technical findings that are preliminary or of specialized interest, e.g., quick release reports, working papers, and bibliographies that contain minimal annotation. Does not contain extensive analysis.

- CONTRACTOR REPORT. Scientific and technical findings by NASA-sponsored contractors and grantees.

- CONFERENCE PUBLICATION. Collected papers from scientific and technical conferences, symposia, seminars, or other meetings sponsored or co-sponsored by NASA.

- SPECIAL PUBLICATION. Scientific, technical, or historical information from NASA programs, projects, and missions, often concerned with subjects having substantial public interest.

- TECHNICAL TRANSLATION. English-language translations of foreign scientific and technical material pertinent to NASA's mission.

Specialized services also include organizing and publishing research results, distributing specialized research announcements and feeds, providing information desk and personal search support, and enabling data exchange services.

For more information about the NASA STI program, see the following:

- Access the NASA STI program home page at http://www.sti.nasa.gov

- E-mail your question to help@sti.nasa.gov

- Phone the NASA STI Information Desk at 757-864-9658

- Write to:
  NASA STI Information Desk
  Mail Stop 148
  NASA Langley Research Center
  Hampton, VA 23681-2199

NASA/TM–2018-219804

A Study of Shape Memory Polymer Based Slat-Cove Filler

Jin Ho Kang
National Institute of Aerospace, Hampton, Virginia

Emilie J. Siochi and Travis L. Turner
Langley Research Center, Hampton, Virginia

Ronald K. Penner and Richard Thomas
Science & Technology Corporation, Hampton, Virginia

Sean Brown
Oregon State University, Corvallis, Oregon

National Aeronautics and
Space Administration

Langley Research Center
Hampton, Virginia 23681-2199

July 2018

Available from:

NASA STI Program / Mail Stop 148
NASA Langley Research Center
Hampton, VA 23681-2199
Fax: 757-864-6500

Abstract

Aircraft noise reduction is an application of current intense interest for which smart materials show significant potential. Specifically, the aeroacoustic noise produced by the unsteady aerodynamic flow about the leading-edge high-lift device, such as leading-edge slat, of typical transport-aircraft wings is of particular interest. Concepts with the most promise to mitigate this noise source, most notably the slat-cove filler concept, have focused on highly reconfigurable structures that change shape between different phases of the flight envelope. These shape changes often involve large deformation, which has stimulated the consideration of shape memory materials. In recent years, shape memory materials (SMMs) have drawn greater interest for applications such as smart fabrics, intelligent medical devices, self-deployable space structures, morphing structures and packaging. Compared to other shape memory materials, like shape memory alloys (SMAs) or shape memory ceramics (SMCs), shape memory polymers (SMPs) have desirable advantages such as high elastic deformation to enable large shape change, broad tailorability of mechanical properties, potential biocompatibility and biodegradability, ductility, light weight and ease of processing. However, SMPs still have some critical disadvantages such as insufficient mechanical and thermal characteristics for structural applications, low recovery stress, and long response time. The new LaRC shape memory thermosetting polymer composite (LaRC-SMPC) discussed herein was synthesized with non-toxic monomers and conductive/magnetic fillers to yield enhanced thermal/mechanical characteristics and faster response times. LaRC-SMPCs with a variety of fiber reinforcements [Kevlar®, carbon fiber (standard and thin-ply), and carbon-nanotube (CNT) sheet] were fabricated to tailor the physical properties and test for suitability as a slat-cove filler (SCF). The performance of SCF prototypes fabricated with the developed LaRC-SMPCs was evaluated using a bench-top test apparatus. The SCFs made of Kevlar® fiber fabric or carbon fiber fabric infused shape memory polymer composite (SMPC) exhibited kinking during simulated deployment and stowage, which can be problematic during operation. The SCF made of CNT sheet/SMP composite did not exhibit kinking, but the deployment was sluggish compared to carbon fiber fabric/SMP composite. This report documents the evolution of designing SMPCs as slat-cove fillers for aircraft noise reduction. In the course of the investigation, several

approaches were investigated to address shortcomings in material characteristics based on performance requirements of operational slat-cove fillers.

1. Introduction

The mission requirements for typical aerospace vehicles usually involve widely-varying operating conditions. However, most aerospace structural systems are point designs, i.e., designed for a single, most-critical operating condition, or they represent a compromise between multiple points on the operational envelope. Examples of this design paradigm are present in most aircraft engine and wing structures. Inlet cowlings and exhaust nozzles for transport-aircraft engines are designed primarily for efficient cruise performance. Performance efficiency in other phases of flight is secondary. While acoustic emissions from jet engines have been a growing concern for many years, engine noise has been addressed primarily by progressively increasing the bypass ratio. Increased bypass ratio increases the percentage of engine exhaust at reduced flow speed, which weakens the mechanisms for noise production, at the expense of greatly increased engine size. The acoustic source strength within the engine is typically treated by passive, absorptive elements that dissipate some of the acoustic energy. This approach has resulted in aircraft engines that have reached limits of practical size and weight, while noise goals continue to become more aggressive.

Similarly, transport-aircraft wing design is driven mainly by cruise efficiency. The cruise-wing size and shape are optimized to produce the required lift with minimum drag at nominal cruise speeds. Desirable cruise wing characteristics typically include a slightly cambered sectional shape to produce the desired lift at low angle of attack (AoA), sweep to delay shock formation at transonic flow speeds, and taper to decrease lift-induced drag. The lift and stall performance of the wing in the approach and landing phases of flight is another important factor in wing design. The low speeds required for landing usually mandate a much higher AoA, increased wing camber and increased wing chord. The typical approach to accommodating these disparate requirements is to use a deployable high lift system.

The high-lift system of typical-transport aircraft usually consists of leading- and trailing-edge devices that are deployed away from the main wing in the high-lift configuration, i.e., separated by gaps, because a multi-element system can sustain a much larger pressure difference (lift) between the upper and lower surfaces than a single wing element with equivalent camber and chord. It is desirable for the multi-element wing to revert to a smooth single-element during the

cruise phase of flight to reduce drag. In current practice, the multiple wing elements are nested together with the leading edge of each element, after the foremost, fitting into the cove in the aft lower surface of the preceding element. A typical arrangement for a three-element airfoil system is shown in retracted (cruise) and deployed (high-lift) configurations in Figure 1 [1].

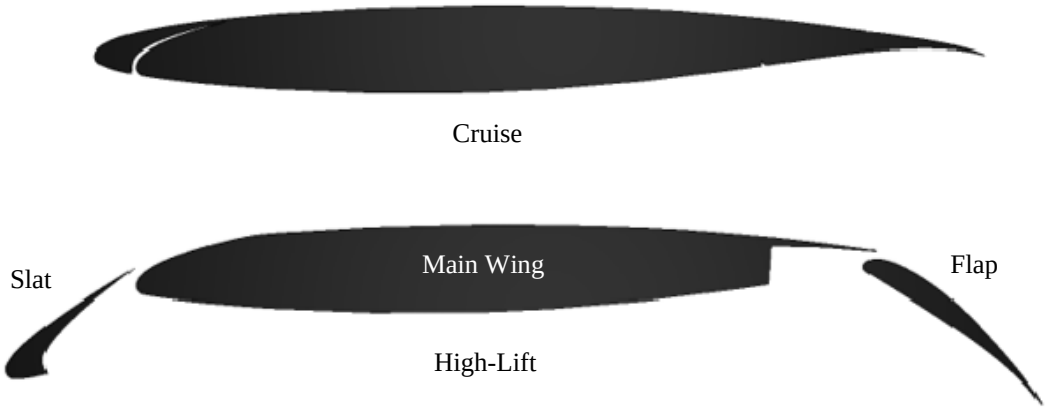

Figure 1. Schematic of a three-element airfoil system in the retracted (cruise) and deployed (high-lift) configurations, adapted from Scholten et al. [1].

The high-lift configuration of the multi-element wing presents many geometric discontinuities, such as edges, gaps and cavities, to the flow. The discontinuities cause considerable unsteadiness in the flow, which is exemplified by the flow vorticity aft of the deployed, leading-edge slat in Figure 2 [2]. The unsteady flow generates significant acoustic noise that radiates outward from the wing and may be heard by observers on the ground below the aircraft [2-6]. Filling the slat-cove, termed a slat-cove filler (SCF), is one method that has been shown, computationally and experimentally, to reduce the unsteady aerodynamics and thus, the aeroacoustic noise associated with the deployed leading-edge slat [7-8]. The SCF concept is the only technology known that significantly reduces the aeroacoustic noise produced by the leading-edge slat while leaving the separated high-lift system intact, with no negative affect on the high-lift or cruise aerodynamic performance.

The SCF profile indicated by the dashed line in Figure 3 is representative of an optimized (for minimum noise) shape based upon the total pressure distribution in the flow field. Part (a) of

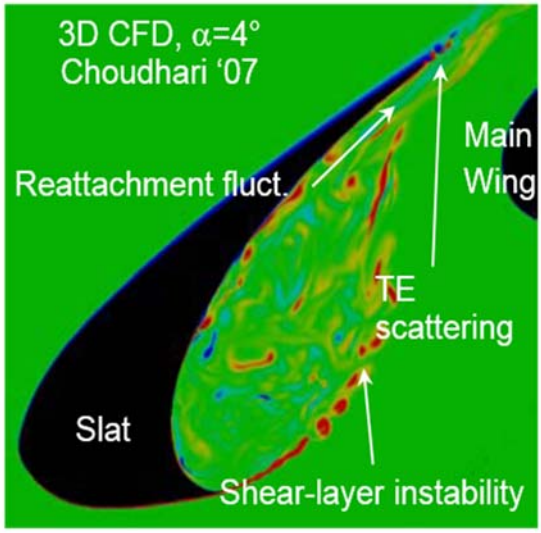

Figure 2. Flow vorticity in the vicinity of the deployed, leading-edge slat [1].

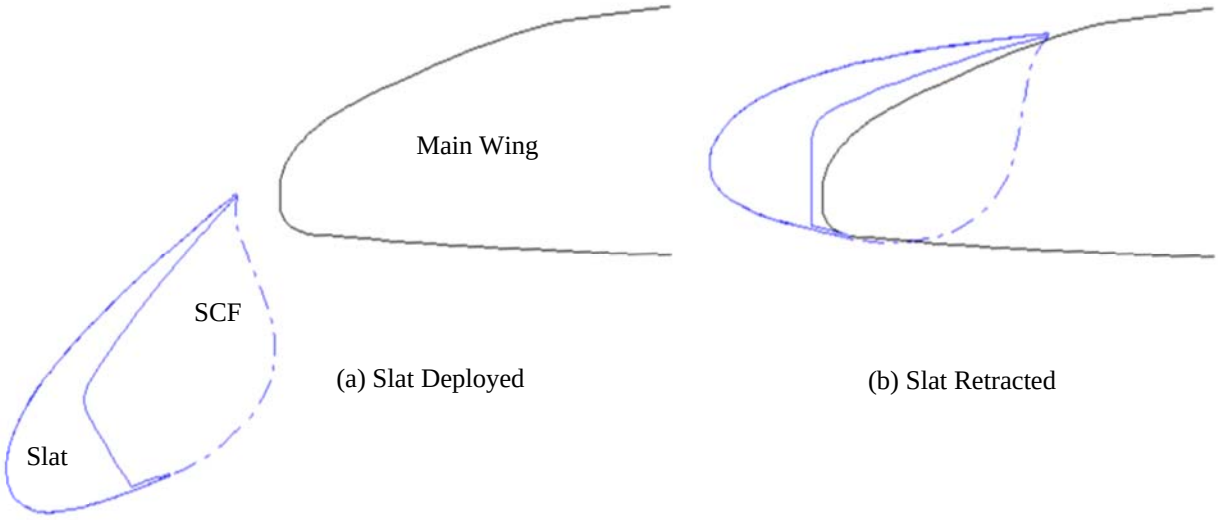

Figure 3. Optimized SCF profile shown (a) on deployed slat and (b) on retracted slat for indication of stowage challenge.

that figure shows the SCF in the deployed configuration along with the slat. Part (b) shows the deployed SCF with the retracted slat, which emphasizes the challenge in stowing the SCF in the small space between the retracted slat and the main wing. Although the SCF profile based upon

total pressure has a greater curvilinear length than profiles based upon other metrics, therefore making it more difficult to stow, it offers the advantage of greater noise-reduction.

The SCF must take the proper shape and sustain the aerodynamic load when deployed, and remain hidden between the slat and main wing when stowed for cruise. Structural and operational characteristics of typical transport aircraft impose constraints on the implementation of a SCF. Additionally, desirable attributes for an effective SCF design include weight-efficiency, passivity (no requirement for auxiliary support systems), durability and fail-safety. A deformable structure that stows in the cavity between the slat and main wing under the authority of the slat actuators and deploys automatically with deployment of the slat, without a dedicated actuation or other support system, was identified as the most efficient and practical design to meet the requirements.

It is clear from Figure 3 that massive reconfiguration of the SCF structure is required to achieve the highly-disparate deployed and retracted configurations. Deforming, mechanized and several combined approaches have been considered for enabling a reconfigurable SCF. A thin, shell-type structure was found to best meet the constraints and requirements [9]. The large-deformation requirement was met through the use of shape memory alloy (SMA) materials [9-11]. The structural concept developed in that work consisted of a thin shell of superelastic-SMA material that is stress free in the shape of the deployed SCF, joined to the slat at the trailing edge in a lap joint and joined to the slat near the cusp by a hinge. A schematic example of that configuration is shown in Figure 4. The contact force developed between the slat-cove filler and the main wing during slat retraction was used to generate the stress required to transform the microstructure in the SCF and achieve the required deformation. The force required for stowage can be minimized by appropriate choice of parameters like hinge length, hinge location, SCF thickness, alloy chemistry and alloy processing and the large deformation requirement is accommodated by the transformation-strain mechanism in the SMA material. Bi-stability can also be avoided by proper choice of parameters, enabling the restoring force to deploy the slat-cove filler autonomously and continuously upon deployment of the slat from the main wing. The hinge is required in the slat-cusp region because of the close-fitting configuration that the slat makes with the main wing at that location when retracted.

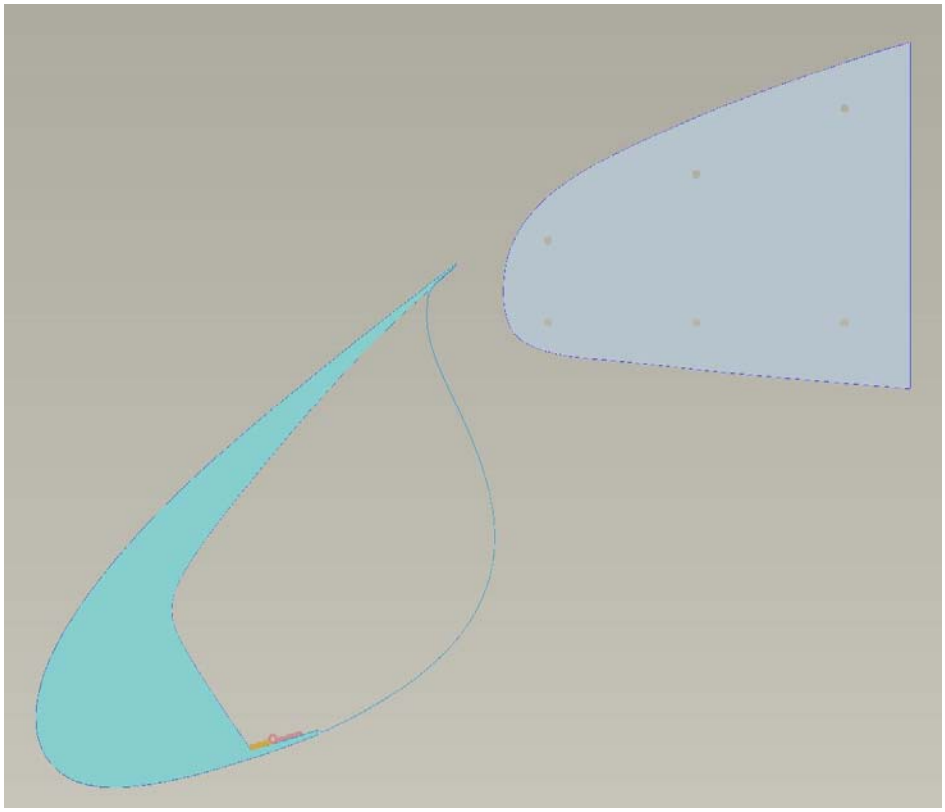

Figure 4. Schematic of a SCF implementation consisting of a single SMA flexure with a lap joint at the slat Trailing Edge (TE) and the hinge joint near the slat cusp.

Although the previous structural concept development work [9-11] achieved proof of concept and included optimization of the structure to minimize the actuator authority required to retract the slat and stow the SCF, contact forces between the SCF and the main wing continue to be a concern in terms of durability, actuation authority requirements, and effects on maintaining the optimized geometry of the main-wing leading edge. It is for these reasons that other material options were sought. Polymer based shape memory materials are of particular interest because they can exhibit dramatic stiffness (modulus) change between states. This characteristic has the potential to significantly reduce contact force/stress, being essentially elastomeric at temperatures above their glass transition while exhibiting structural stiffness below the glass transition temperature.

Shape memory polymers (SMPs) have been studied due to their intrinsically high elastic deformation (broad tailorability of mechanical properties), potential biocompatibility and biodegradability, ductility, light weight and ease of processing [12-14]. Polyurethane based SMP (Diaplex®) is the most common commercial product [15]. State of the art SMPs still have critical disadvantages for the SCF application. They have insufficient mechanical and thermal characteristics for structural applications, a low recovery stress, and slow response time of about a minute. For example, a polyurethane based shape memory polymer (32mm × 7mm × 1 mm rectangular specimen) recovered its original unfolded shape in about 30 - 40 seconds with a 90°C change in temperature [16]. An epoxy based shape memory polymer (250mm × 25mm × 2 mm rectangular specimen) recovered its original unfolded shape in about 2 minutes when subjected to a 100°C change in temperature [17].

Recently, some thermosetting epoxy shape memory polymers were developed [18] that satisfy high mechanical and temperature requirements. The transformation temperature of these epoxy based SMPs is about 60ºC. This temperature is tailorable by adjusting monomer stoichiometries. To increase recovery stress, some fillers like glass fibers and silicon carbide fibers were incorporated [19-20]. Adding conductive or magnetic fillers like carbon black, carbon fibers, carbon nanotubes or nickel particles into SMPs were approaches attempted to improve response time via electroactive triggering [21-23].

Despite the methods used to overcome shortcomings of shape memory materials, they still have poor mechanical strength, durability and slow response time (about 30 seconds ~ 1 minute). These characteristics make them unsuitable for the SCF application which requires endurance for aerodynamic loading during operation. Adding conductive fillers yielded limited improvements in shape transformation response because they exploited only Joule heating. Furthermore, the epoxy-based SMP [18] utilizes a highly volatile and toxic monomer, so it requires a closed mold during processing that restricts the versatility of composite configurations.

The following operational conditions and constraints guided the SMP development work in this study. The deployed SCF must sustain the steady aerodynamic load of a typical approach and landing flow condition (Mach 0.2 and angle of attack of 6-8 degrees) with an acceptable deflection. Previous work suggests that a deflection of 3.39 mm represents an acceptable deviation from the desired aerodynamic shape for maximum noise reduction with a typical

transport aircraft at full scale [9]. The SCF structure must also endure mechanical strains potentially to 2% for as many as 70,000 (pressurization) cycles, although fatigue performance is outside the scope of this study. The SCF must soften during retraction of the slat with the goal of reducing the contact stress between the SCF and the main wing, relative to the baseline SMA SCF, so as to improve durability of the SCF system and reduce the actuator requirements for stowage. The time to soften during retraction must be shorter than the typical retraction time of a slat, which was taken to be in the range of 10-20 seconds. Additionally, static and dynamic stability of the SCF structure to the aerodynamic load is required at all times, but this is beyond the scope of this study. Finally, the SCF should reacquire the deployed shape and rigidize during deployment of the slat/SCF to within 0.34 mm of the optimized configuration for noise reduction. The deployment of the SCF should be timed such that it achieves an aerodynamically and aeroacoustically suitable shape as the SCF loses contact with the main wing during slat deplomen. Thus, the time required to recover from the stowed configuration to the deployed, permanent configuration should be similar to the slat deployment time of 10-20 seconds. It is clear that chordwise staging of the heating and cooling of the structure could be beneficial to the performance during retraction and deployment of the slat/SCF, particularly in terms of aeroelastic stabiltiy of the SCF. However, this is not known to be a requirement.

The above parameters provided guidance for performance targets required for a material system to be considered as a SCF. Physical properties (modulus, electrical conductivity, shape transformation response) were controlled by tailoring molecular structure with different monomers and doping with nanoinclusions [carbon nanotubes (CNTs), functionalized graphene sheets (FGS)]. To improve mechanical durability and stiffness, Kevlar® or carbon fiber was incorporated in the SMP matrix. The strategy used in the development of shape memory polymer based slat-cove filler is shown in Figure 5. The material designs developed were evaluated based on the operational requirements of SCFs. New SMP compositions were developed to meet the required physical properties. When the new material satisfied the desired properties, a prototype SCF was fabricated to demonstrate the actuation. Details of the lessons learned from exploring various SMPC compositions will be discussed.

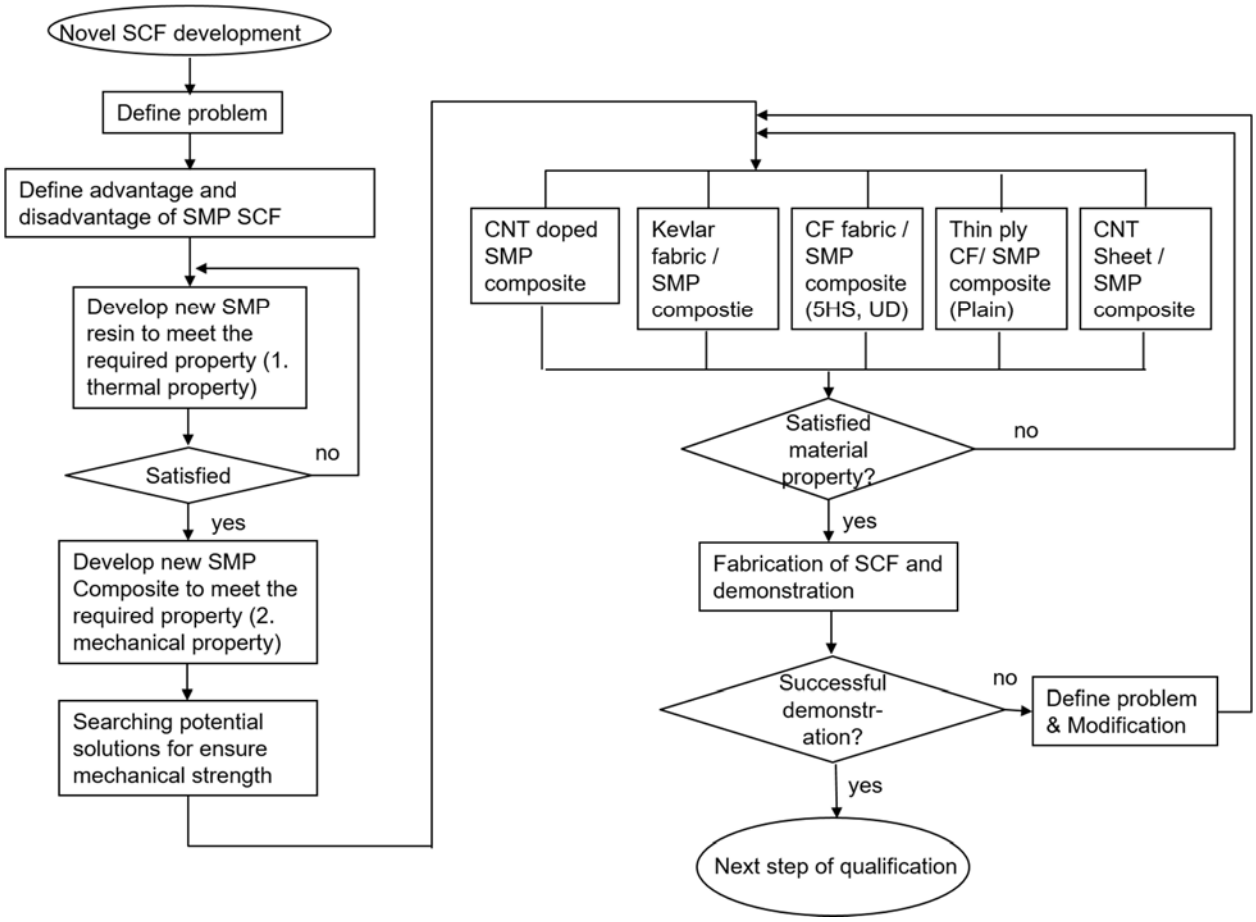

Figure 5. Research strategy for development of shape memory based slat-cover filler.

2. Experiments

2.1. Materials

Diglycidyl ether of bisphenol A diglycidyl ether (DGEBA), Araldite® 506, poly(bisphenol A-co-epichlorohydrin), benzhydrylamine (BZA), (3-glycidyloxypropyl)trimethoxysilane (GPTS) and (3-aminopropyl)trimethoxysilane (APTS) were purchased from Aldrich Chemical Co. and used without further purification. 3,4'-oxydianiline was purchased from Mitsui Petrochemical, Ind., and used without further purification. Functionalized graphene sheet (FGS, Vor-x™) was obtained from Vorbeck Materials and used in the as-received condition. Multiwall carbon

nanotubes (MWCNT) were obtained from Duke University and used in the as-received condition. Poly(n-butylene oxide)-b-poly(ethylene oxide) [PBO-PEO diblock copolymer (PBE)] was obtained from Dow Chemical and was used as a toughening agent without further purification.

2.2. Synthesis of new NASA Langley Research Center shape memory polymer (LaRC-SMP)

Epoxy-based thermosetting shape memory polymer (SMP) resin was synthesized with diglycidyl ether of bisphenol A (DGEBA) as a resin and aromatic amines (benzyldrylamine (BZA) and 3,4'-oxidianiline (ODA) as the curing agents. The molar ratio of epoxide equivalent to amine was 1:1. For example, 2.5 mmol of ODA and 5 mmol of BZA were mixed to 10 mmol of DGEBA to get equivalent molar ratio between epoxide and amine functional groups. The mole ratios of ODA to DGEBA were 0, 0.025, 0.1, 0.25 and 0.5. The precursors were mechanically premixed and a predetermined amount of PBE was added to the resin. The premixed resin was placed in a mixing apparatus consisting of a temperature-controlled sonication bath and a mechanical stirrer.

2.3. Fabrication of NASA Langley research center shape memory polymer composites (LaRC-SMPC)

In order to fabricate a shape memory polymer based slate-cove filler, five LaRC-SMPCs were fabricated as shown in Figure 5. Reinforcements used included: (1) Carbon nanotube (CNT) or functionalized graphene sheets (FGS) doped SMPC; (2) Kevlar® fabric/SMPC; (3) Carbon Fiber (CF)/SMPC; (4) Thin ply CF/SMPC; (5) CNT sheet/SMPC. To make CNT or FGS doped SMPCs, a predetermined amount of CNT or FGS was mixed with the resin under high shear at 60°C and 25 kHz sonication for 2 hours. To make fiber reinforced SMPC, the resin was painted on the fabric (Kevlar®, regular CF, thin ply CF or CNT sheet) to produce fiber/SMPC prepreg. The fiber/SMPC prepreg sheets were stacked and cured in an autoclave (heating rate of 2°C/min, 30 minutes at 100°C and 150°C, each, 4 hours at 175°C, 0.10 – 0.69 MPa).

2.4. Characterization

Tensile properties of film were characterized according to ASTM standard D882-12 [23]. Specimens (5 mm wide) were placed between grips with a gauge length of 50 mm and pulled at a rate of 5 mm/minute until failure. Viscoelastic behavior of the LaRC-SMPC was determined using a dynamic mechanical analyzer (DMA Q800, TA Instruments). Storage and loss moduli were determined at 1 Hz using a heating rate of 1°C/min. A Hitachi S-5200 high-resolution scanning electron microscope (HRSEM), with a field emission electron gun and in-lens detector, was used to examine the surface morphology of the samples. Infrared (IR) spectra were taken in transmission mode with a Fourier Transform Infrared (FT-IR) spectrometer (Nicolet iS^{TM} 5).

2.5. Bench-top demonstration model development

A bench-top test apparatus, based on the 30P30N airfoil, was developed at 75% scale to assess the operational viability of the LaRC-SMPC based slat-cove filler (SCF) prototypes as shown in Figure 6 [9-10]. The bench-top apparatus is approximately 45 cm in length and ball-bearings were mounted beneath the slat that moved within slots of the baseplate to enforce proper kinematics. The performance of different LaRC-SMPC based SCFs was investigated and recorded by a digital camera.

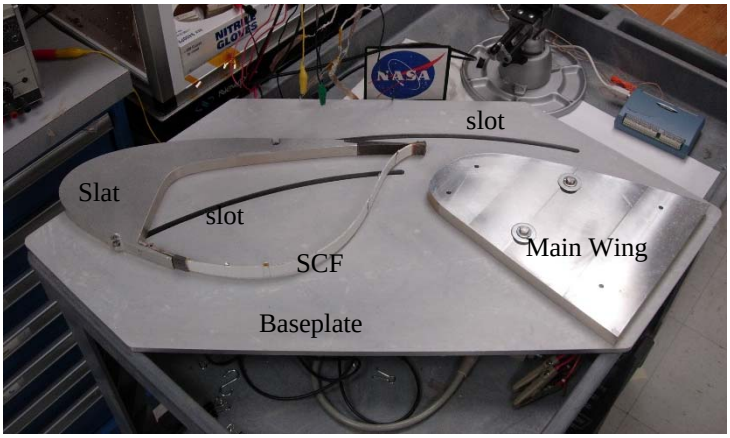

Figure 6. Bench-top demonstration model for feasibility test of LaRC-SMP SCF.

3. Results and Discussion

3.1. New LaRC Shape Memory Polymer Composite

3.1.1. Synthesis of new LaRC shape memory polymer resin

Two different epoxy based SMPs were synthesized: DGEBA based SMP and Araldite® 506 based SMP. The glass transition temperature of SMPs synthesized with different mole ratios of ODA to DGEBA (0, 0.025, 0.1, 0.25 and 0.5) are shown in Figure 7. The glass transition temperatures of DGEBA based SMPs varied from 90°C to 170°C, depending on the mole ratio of BZA used [Figure 7 (a)]. When more flexible monomer of Araldite® 506 was used, the glass transition temperature decreased and varied from 60°C to 140°C [Figure 7 (b)]. The sample cured on an open Teflon plate showed higher glass transition temperature compared to the sample cured in a closed Teflon mold. Because the prepared pristine SMP was too insulating to exhibit a fast response to external thermal and electrical energy, conductive nanoparticles were incorporated into the SMP matrix. Because the glass transition temperature of about 100°C is appropriate for our application, and DGEBA is widely used as a epoxy resin, we chose the mole ratio of ODA to DGEBA of 0.1 for futher study.

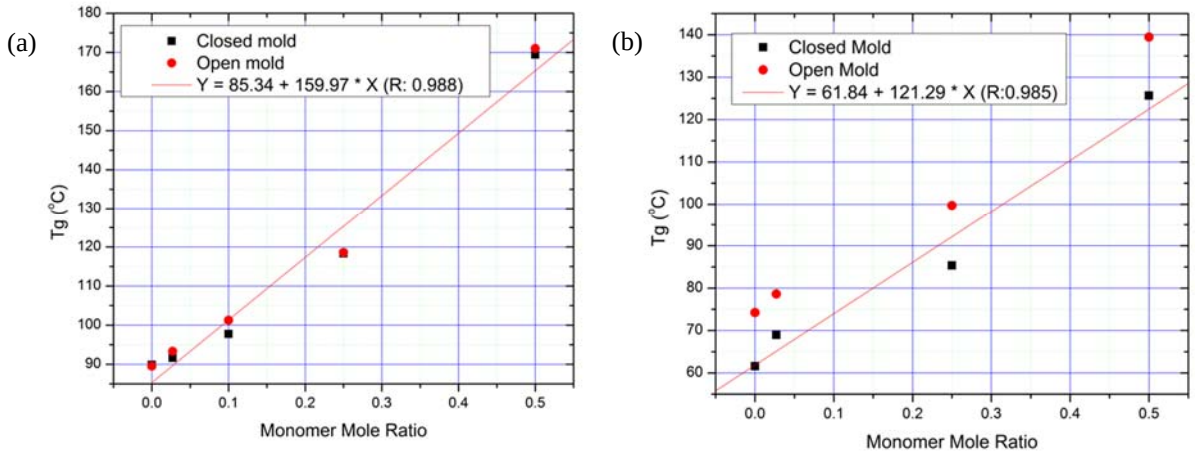

Figure 7. Glass transition temperature of (a) DGEBA based LaRC-SMP and (b) Araldite® 506 based LaRC-SMP.

3.1.2. LaRC shape memory polymer composite 1 (Carbonaceous nanophase doped SMP).

To increase electric conductivity, carbonaceous nanophase materials like CNT or FGS were added to pristine LaRC-SMP. The mole ratio of ODA to DGEBA was 0.1. The glass transition temperatures (T_g) of the pristine-SMP and the LaRC-SMPC were about 98ºC and 97ºC, respectively, measured by a DSC. Figure 8 shows thermo-mechanical properties of pristine LaRC-SMP and LaRC-SMPC. Tensile tests were done at room temperature and elevated temperature (T_g + 30ºC), respectively. Pristine LaRC-SMP displayed a high elastic modulus of 2.8 GPa and a relatively low tensile strain at break of about 6.3% at room temperature. It exhibited a low elastic modulus of only 7.5 MPa and a high tensile strain at break of higher than 38% [Figure 8 (a)] above the glass transition temperature (T_g + 30ºC). The drastic change of elastic modulus of LaRC-SMP with temperature change is a critical parameter for making a variable stiffness material. The LaRC-SMPC behaves in a similar fashion as pristine LaRC-SMP. The addition of 2 wt% commercial FGS did not result in any improvement of mechanical properties.

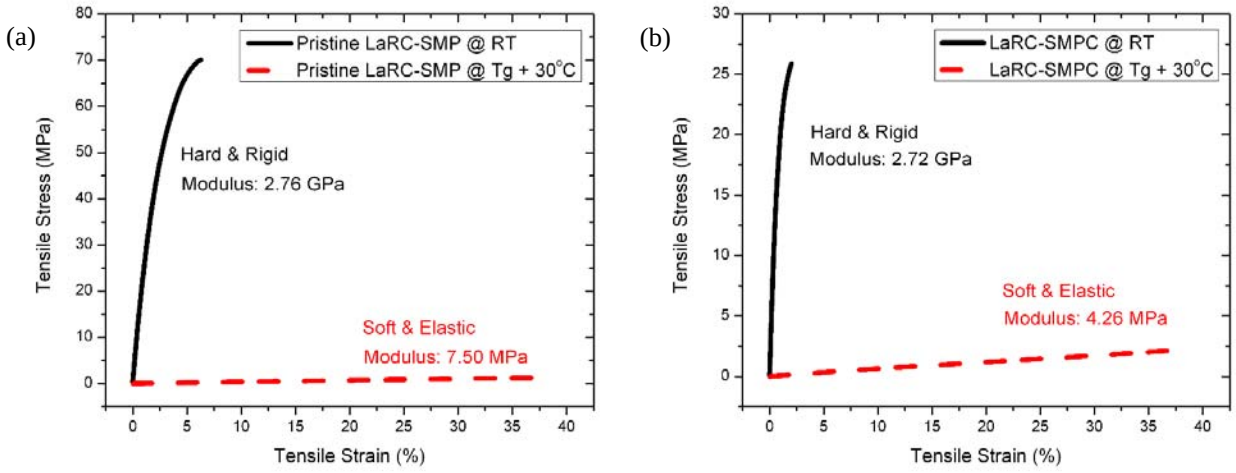

Figure 8. Mechanical properties measured at room temperature and at elevated temperature (30°C above the glass transition temperature) of (a) pristine LaRC shape memory polymer (LaRC-SMP) and (b) LaRC shape memory polymer composite (LaRC-SMPC, 2% FGS doped).

Real dielectric constant and real AC conductivity of LaRC-SMPC are shown in Figure 9. LaRC-SMPC exhibited higher dielectric constant than pristine LaRC-SMP, and had a large

dielectric relaxation as a function of frequency [Figure 9 (a)]. Pristine LaRC-SMP showed lower AC conductivity with a conventional insulator's trend with increasing frequency, whereas conductive filler doped LaRC-SMPC exhibited higher conductivity with a conventional conductor's trend with increasing frequency.

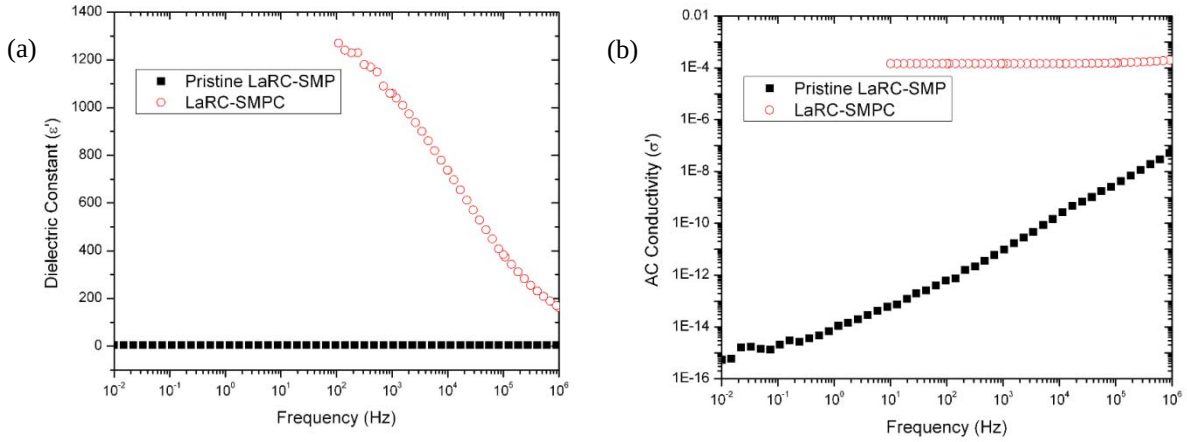

Figure 9. (a) Dielectric constant and AC conductivity of pristine LaRC-SMP and LaRC-SMPC.

In order to trigger the shape reformation, the temperature of the material needs to be above its glass transition temperature. In order to decrease response time, electric power input was employed to increase the temperature of the material internally, via internal heat generation, instead of superficially, via applied surface heaters. The temperature of the LaRC-SMPC was monitored with an IR camera while direct current (DC) voltage or alternating current (AC) voltage, in the frequency range from 0.1 Hz to 1 MHz, was applied to the specimen (Figure 10). The temperature response of LaRC-SMPC depended on the polarity change of the applied electric field (DC or AC) and the frequency of excitation. At the frequencies of 0.1 and 10 Hz, the applied AC electric field caused faster heating than the applied DC electric field. At a frequency of 1 kHz, the heating became slower than the lower frequencies of 0.1 and 10 Hz, but it still showed faster heating than the DC electric field. Above 1 kHz, heating augmentation of the alternating field continues to diminish until it eventually results in a heating rate deficit such that at a frequency of 10 kHz, the heating was significantly slower than the DC electric field. Further, no significant electric field induced heating was observed at the highest frequency of 1

MHz. The high heating augmentation at the low frequencies (0.1 Hz ~ 1 kHz) of applied AC electric field seemed to orginate from the dielectric loss heating due to the high interfacial polarization. Dipoles of interfacial polarization do not repond at excitation frequencies significantly above 1 kHz, resulting in no heating augmentation above the DC field. Furthermore, AC field excitation significantly above 1 kHz also exhibits reduction in effectiveness of Joule heating until no measureable heating of the sample was observed at 1 MHz. This suggests that the synergistic effects from combining loss heating (AC voltage at low

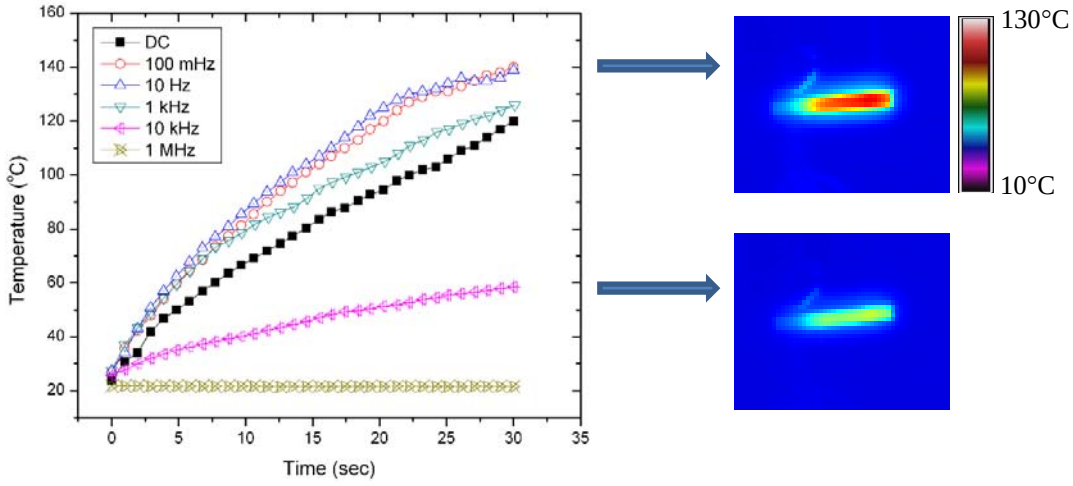

Figure 10. Temperature change of LaRC-SMPC under applied DC and AC electric field.

frequency) and Joule heating (DC voltage) can trigger of shape reformation more effectively.

Figure 11 shows variable stiffness capability of the LaRC-SMPC by applying an electric field. The specimen was placed between compressive grips, and the compressive stress was monitored at constant compressive strain (0.2%) while applying an electric field. The compressive stress increased slightly with increasing applied electric field until a critical transition point, about 15 kV/m for this test specimen. The increase in the compressive stress seems to originate from thermal expansion due to heating under the applied electric field. With further increase of the electric field, the compressive stress dramatically dropped to transform the material from a hard state to a soft state.

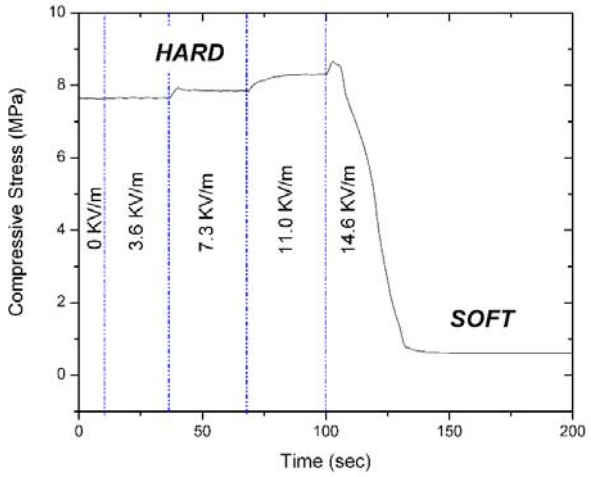

Figure 11. Mechanical stiffness change of LaRC-SMPC under applied DC electric field.

Figure 12 presents the visual demonstration of shape memory effect for LaRC-SMP and LaRC-SMPC. The programmed temporary shape of pristine LaRC-SMP [Figure 12 (a)] returned to the original permanent shape by external thermal heating [Figure 12 (b)]. A full process of thermal shape memory effect is shown in the Appendix (Figure S2) and Reference 21. Figure 12 (c) and (d) show electric field induced shape memory effect. The programmed temporary shape of the LaRC-SMPC [Figure 12 (c)] returned to the original permanent shape by applying an external electric field [Figure 12 (d)]. A visual demonstration video of the shape memory effect is available at NASA Technical Reports Server (NTRS) [24].

The response time of the shape memory effect was measured by monitoring actuation displacement using a fiber optic sensor (Angstrom Resolver^{TM} Model 201, Acousto-Optic Sensors Inc.) as shown in Figure 12 (c) and (d). The response time of LaRC-SMPC was improved by laminating an elastic titanium sheet as shown in Figure 13. The final reformation time (τ_f) from temporary shape to original permanent shape of the LaRC-SMPC laminated with the elastic titanium alloy sheet was about 10.8 sec. This is much faster than that of an unlaminated LaRC-SMPC (τ_f ~ 37.8 sec) and meets the requirement for the ideal response time of about 10 ~ 20 sec for the slat actuation. An increased recovery stress can be expected with a higher stored elastic energy of the titanium alloy sheet.

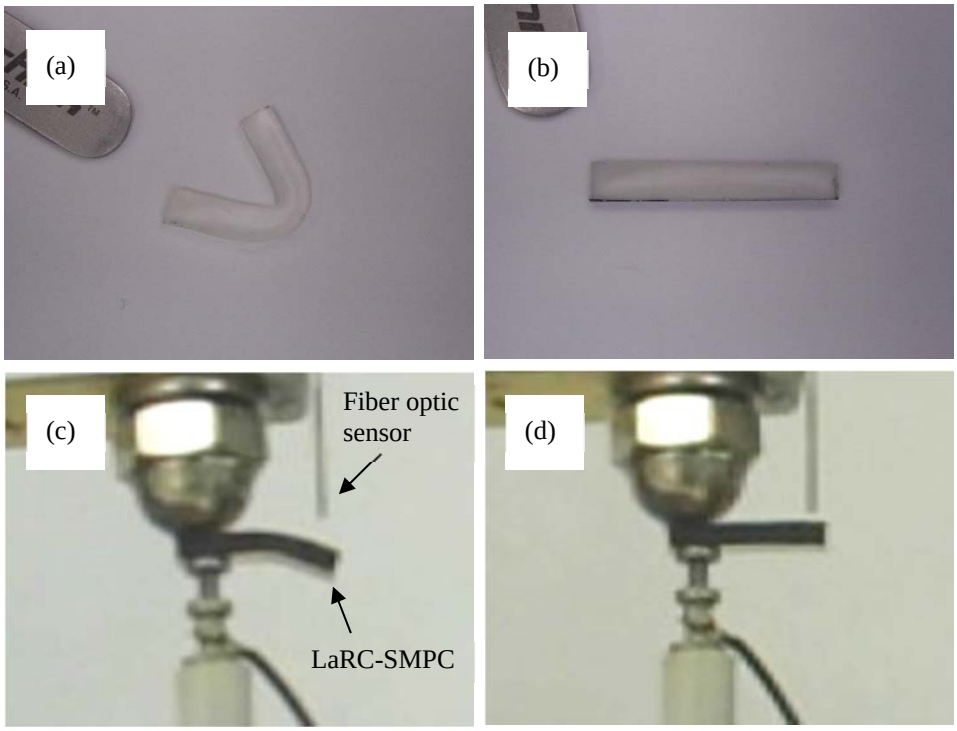

Figure 12. Shape memory effect: (a) programmed temporary shape of pristine LaRC-SMP and (b) original shape of pristine LaRC-SMP recovered by external thermal radiation; (c) programmed temporary shape of LaRC-SMPC and (d) original shape of LaRC-SMPC recovered by external electric field.

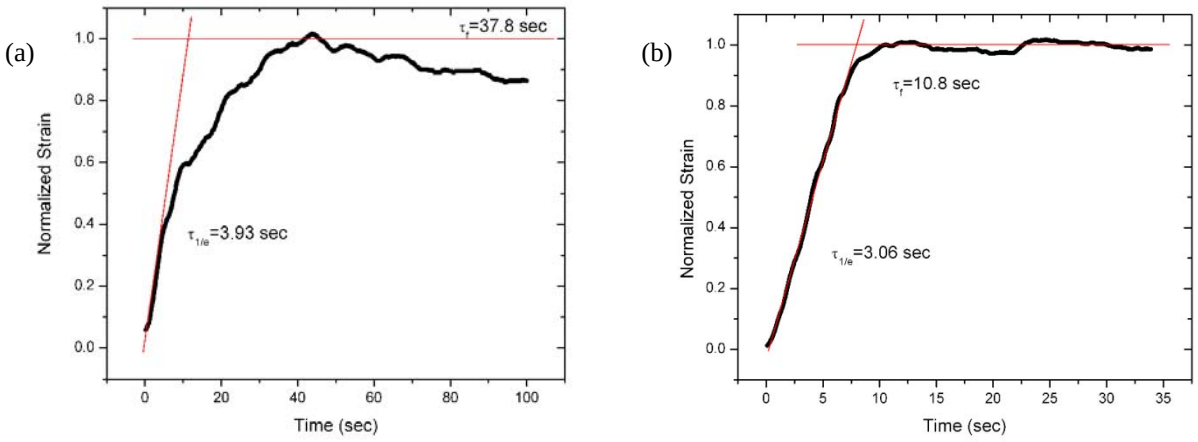

Figure 13. Response time of (a) conventional metal electroded LaRC-SMPC and (b) elastic titanium sheet plated LaRC-SMPC.

3.1.3. LaRC shape memory polymer composite 2 (Kevlar® fiber doped SMP).

The thickness of the slat-cove filler is about 1 mm for the bench-top demonstration (75% scale) and it was found that the mechanical strength of CNT or FGS doped SMP composite was insufficient to endure a mechanical load during operation. Therefore, various fiber reinforced composites were considered as candidates. First, Kevlar® fiber (2×2 twill weave, $[0°/90°]_{3s}$) embedded SMP composite was fabricated to secure mechanical strength. Figure 14 shows the storage modulus as function of temperature of Kevlar® fiber reinforced SMP composite fabricated at different processing condition of pressure (0 to 100 psi) and measurement direction.

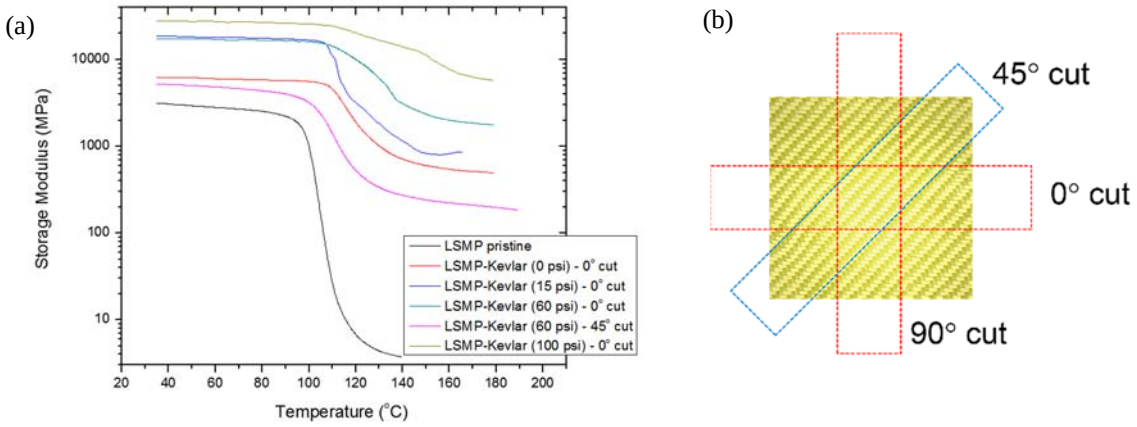

Figure 14. (a) Thermal mechanical properties of Kevlar Fiber/SMP composite and (b) test direction.

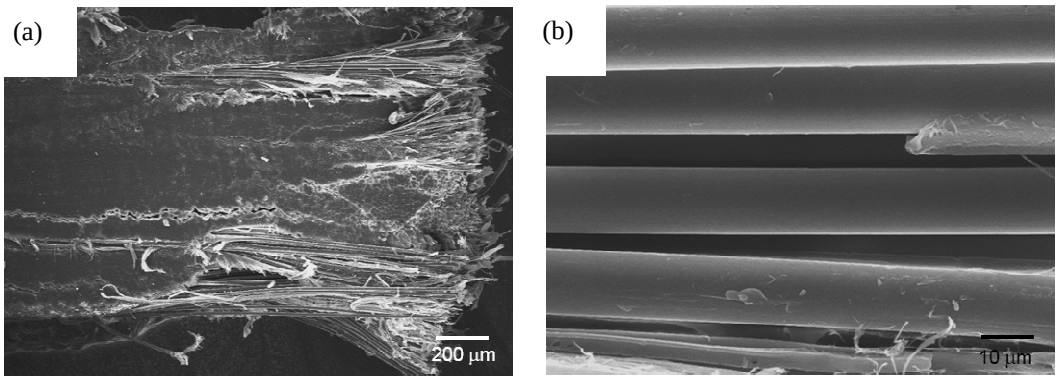

Figure 15. Cross-sectional SEM images of Kevlar® fabric reinforced SMP composite.

The storage modulus below its glass transition temperature increased with increasing processing pressure. The sample cut in the 45° fiber direction shows lower storage modulus compared to 0° sample. However, poor interfacial interaction between Kevlar® fiber and SMP resin was found to result in low mechanical durability. Figure 15 shows the dry Kevlar® fibers on the fracture surface. This is evidence of poor interfacial strength between Kevlar® fiber and SMP resin.

3.1.4. LaRC shape memory polymer composite 3 (Carbon fiber fabric/SMP composite).

For better wettability and high interfacial strength between fibers and SMP resin, uni-directional (UD) and woven (5HS) carbon fiber (CF, IM7, Hexcel) fabrics were employed to make CF/SMP composites. Uni-directional and quasi-isotropic layup configurations were used to investigate the anisotropic mechanical properties. Compared to the Kevlar® fabric reinforced SMP composite, CF/SMP composites showed better wettability of resin on the CF surface after fracture, which implies the stronger interfacial strength between CF and SMP resin (Figure 16). Figure 17 shows dynamic mechanical analysis of UD CF ($[0°]_8$)/SMP composite. The UD layup composite exhibited anisotropic mechanical properties. The sample cut 0° along the fiber direction showed storage modulus of about 108.9 GPa at room temperature while the 90° cut sample modulus was about 7.3 GPa. At the elevated temperature of 125°C, the storage moduli of 0° cut and 90° cut samples decreased to about 47.8 GPa and 0.25 GPa, respectively. The glass

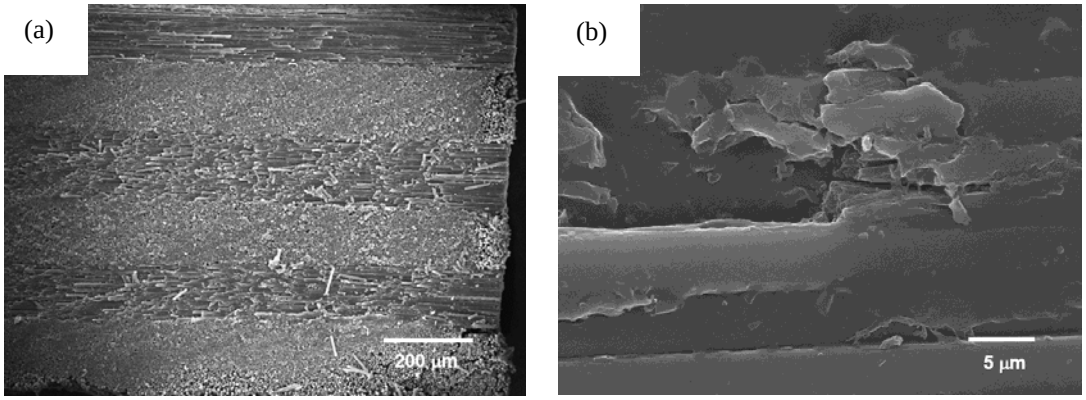

Figure 16. Cross-sectional SEM images of carbon fiber reinforced SMP composite.

transition temperature of the 0° cut sample, determined by a peak of Tan δ, was higher than that of the 90° cut sample (about 93.2°C versus about 79.8°C).

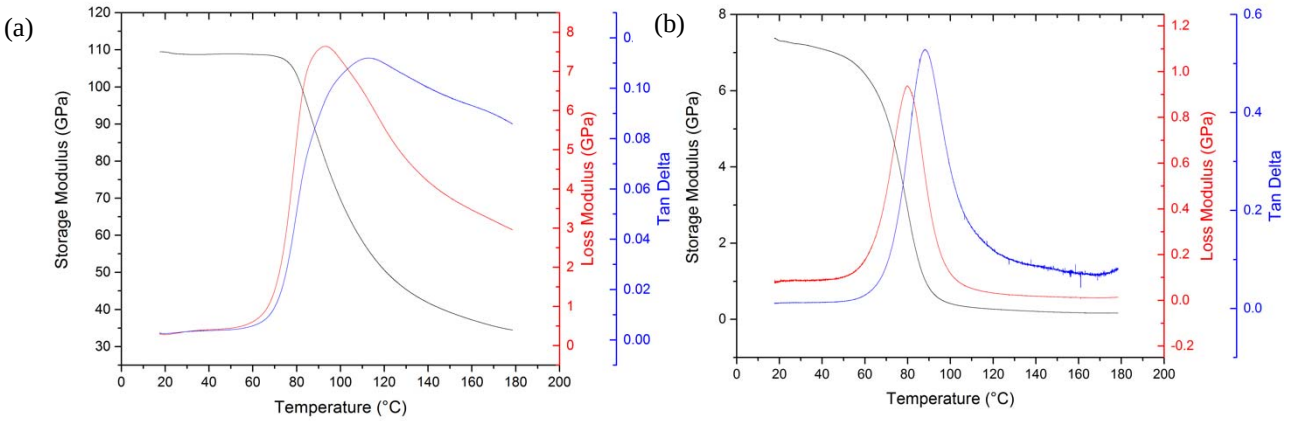

Figure 17. Dynamic mechanical analysis of carbon fiber (UD, $[0°]_8$) reinforced SMP composite of (a) 0° cut and (b) 90° cut.

Figure 18 shows dynamic mechanical analysis of quasi-isotropic CF ($[+45°/0°/-45°/90°]_{2s}$)/SMP composite. The quasi-isotropic layup composite displayed less anisotropy in mechanical properties compared to the unidirectional layup configuration. 0° cut and 90° cut

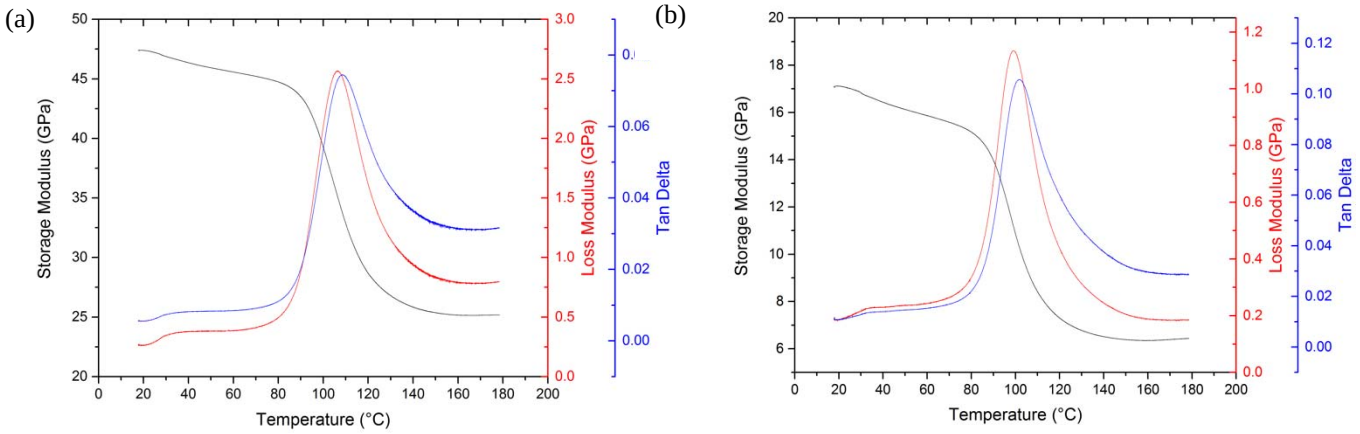

Figure 18. Dynamic mechanical analysis of carbon fiber ($[+45°/0°/-45°/90°]_{2s}$) reinforced SMP composite of (a) 0° cut and (b) 90° cut.

specimens had storage moduli of about 47.2 GPa and 17.0 GPa at 25°C. At the elevated temperature of 125°C, the storage moduli of 0° cut and 90° cut decreased to about 27.9 GPa and 7.0 GPa, respectively. The glass transition temperature of the 0° cut sample, determined by a peak of Tan δ, was higher than that of 90° cut specimen (about 106°C versus about 99°C).

3.1.5. LaRC shape memory polymer composite 4 (CNT sheet/SMP composite).

CNT sheet was employed to reinforce the SMP composite because it is more flexible than carbon fiber and its stiffness is tailorable depending on post processing methods such as stretching of the CNT sheet. Figure 19 shows a dynamic mechanical analysis of a CNT sheet $([0°]_2)$/SMP composite. Storage modulus was about 11.8 GPa at room temperature, 8.2 GPa at 125°C and 5.1 GPa at 175°C. Loss modulus appeared as a clearer peak of glass transition of about 115°C while tan δ increased as a function of temperature.

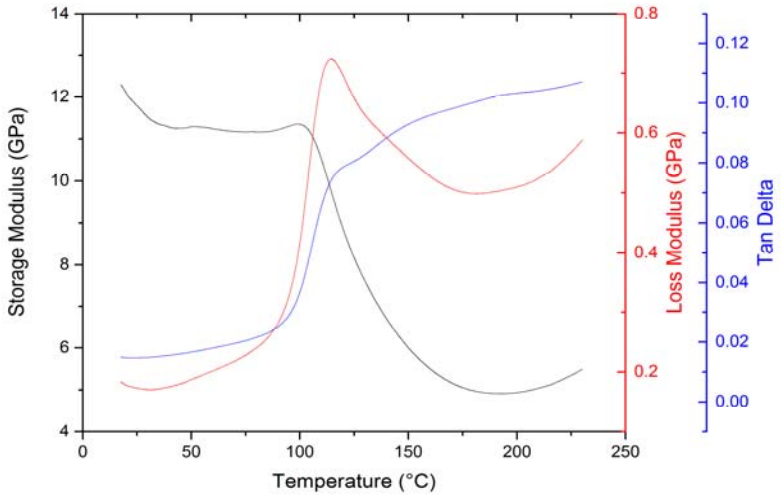

Figure 19. Dynamic mechanical analysis of CNT sheet/SMP composite.

Because the mechanical properties of the CNT sheet/SMP composite were inferior to the CF/SMP composite, the fabrication process of CNT sheet/SMP composites was modified. In order to increase interfacial strength between CNTs and SMP resin, CNT sheets were modified by three different methods: (1) thermal treatment at 250°C for 1 hr, (2) sizing treatment (epoxy

based sizing material, Adherent Technology) without thermal treatment, and (3) sizing treatment (epoxy based sizing material, Adherent Technology) after thermal treatment at 250°C for 1 hr. Figure 20 shows the effect of process condition on the mechanical properties of CNT sheet/SMP composites. The tensile modulus of pristine CNT sheet/SMP composite was about 12.3 GPa. The thermal treatment and sizing treatment increased the modulus up to 13.5 ~ 15.7 GPa. The maximum tensile strength also increased following the thermal and sizing treatment. Compared to the pristine CNT sheet/SMP composite which has elongation at break of about 2.6%, the thermally treated CNT composite showed sligthly higher tensile strain of about 3.4% while the

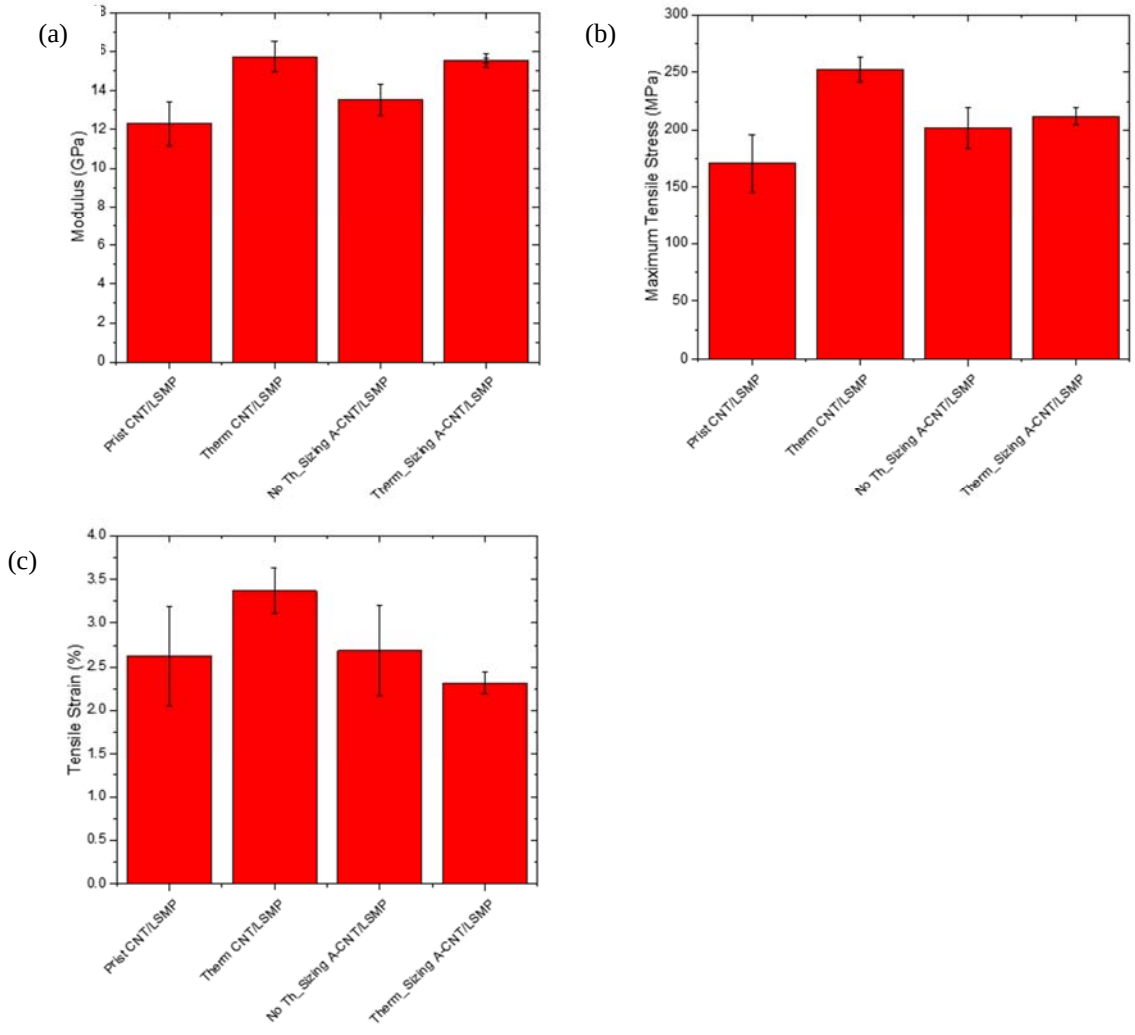

Figure 20. Mechanical properties of CNT sheet/SMP composites. (a) Tensile modulus, (b) maximum tensile strength and (c) elongation at break.

thermally treated and sized composite did not show any significant positive influence on tensile strain. Figure 21 shows the cross-sectional image of thermally treated CNT sheet ($[0°]_{18}$)/SMP composites. It reveals good interfacial interaction between CNT and SMP resin.

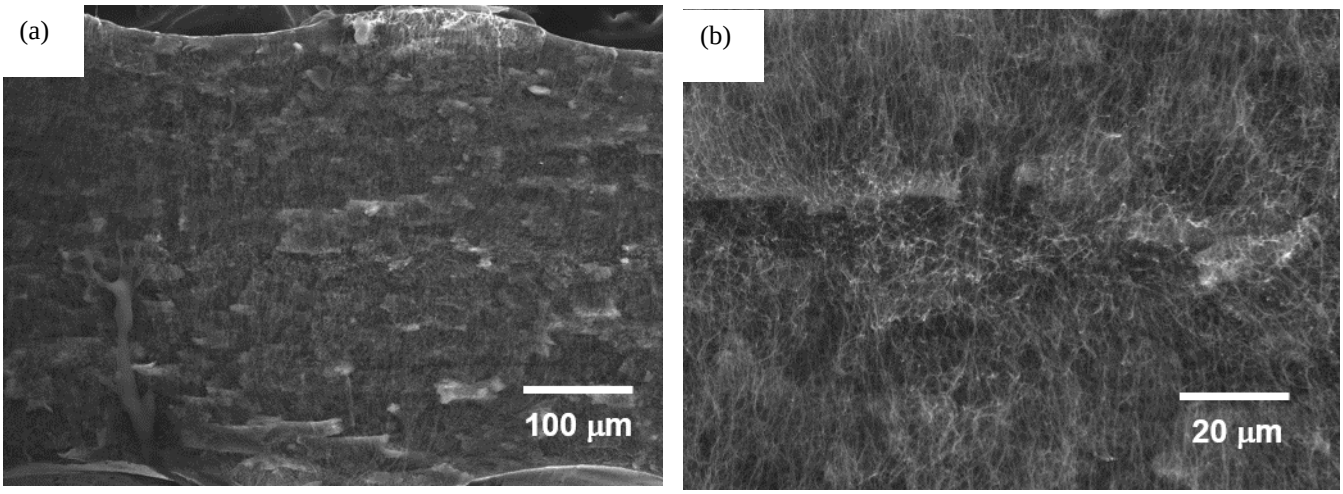

Figure 21. Cross-sectional SEM images of CNT sheet/SMP composite.

3.2. Designing SCF conformation by computational modeling.

Using the Abaqus finite element analysis program, SCF dimensions and the segmented (top, mid-link and bottom section) configuration from previous work, the design of the SCF incorporating the SMP material was studied (Figure 22). The homogeneous SCF without a mid-link showed a failure in deployment (Figure 23). Therefore, high stiffness of mid-link was incorporated for autonomous deployment. The location and size of mid-link were optimized to enable successful retraction/deployment. When the mean mid-link location was about 12.7 to 19.5 cm (5 to 7.5 inches) from the bottom and the mid-link length is about 2.54 to 12.7 cm (1 to 5 inches), the SCF showed good retraction/deployment performance. Figure 24 shows the failure in deployment when the mean mid-link location is 10.16 cm (4 inches) from the bottom and the length is 10.16 cm (4 inches). Figure 25 shows the successful deployment when the mean mid-link location was 16.51 cm (6.5 inches) and length is 7.62 cm (3 inches). Animation results of the computational modeling of SCF are available at NASA Technical Reports Server (NTRS) [25-27]. The optimization results for the mid-link are summarized in Figure 26. A The maximum

strain during retraction/deployment was calculated for the various mid-link locations and sizes (Figure 27). Because the preferred maximum strain is below 2% for composite materials, the optimized mid-link location and size was about 15.24 to 19.05 cm (6 to 7.5 inches) and about 3.81 to 12.7 cm (1.5 to 5 inches), respectively. The optimized paprameters were employed for the fabrication of SCF.

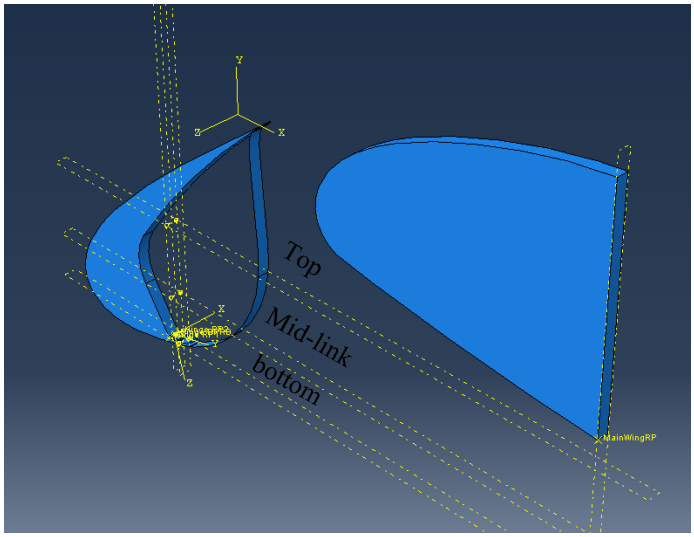

Figure 22. Abaqus model of SCF for retraction/deployment performance.

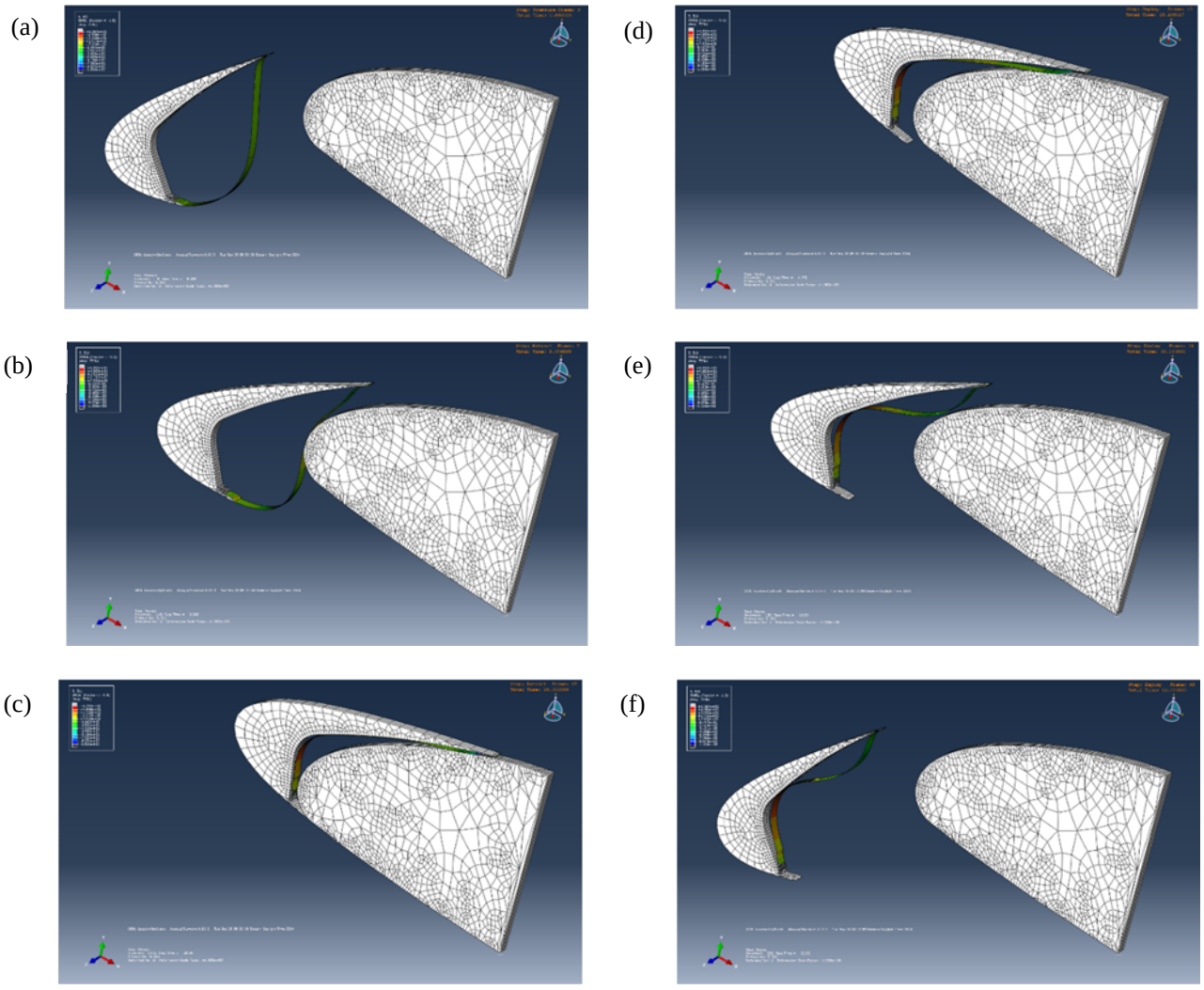

Figure 23. Computation modeling of SMP SCF actuation shows unsuccessful deployment with no mid-link. (a –c) retraction, and (d-f) deployment. A full animation is available at NTRS [22].

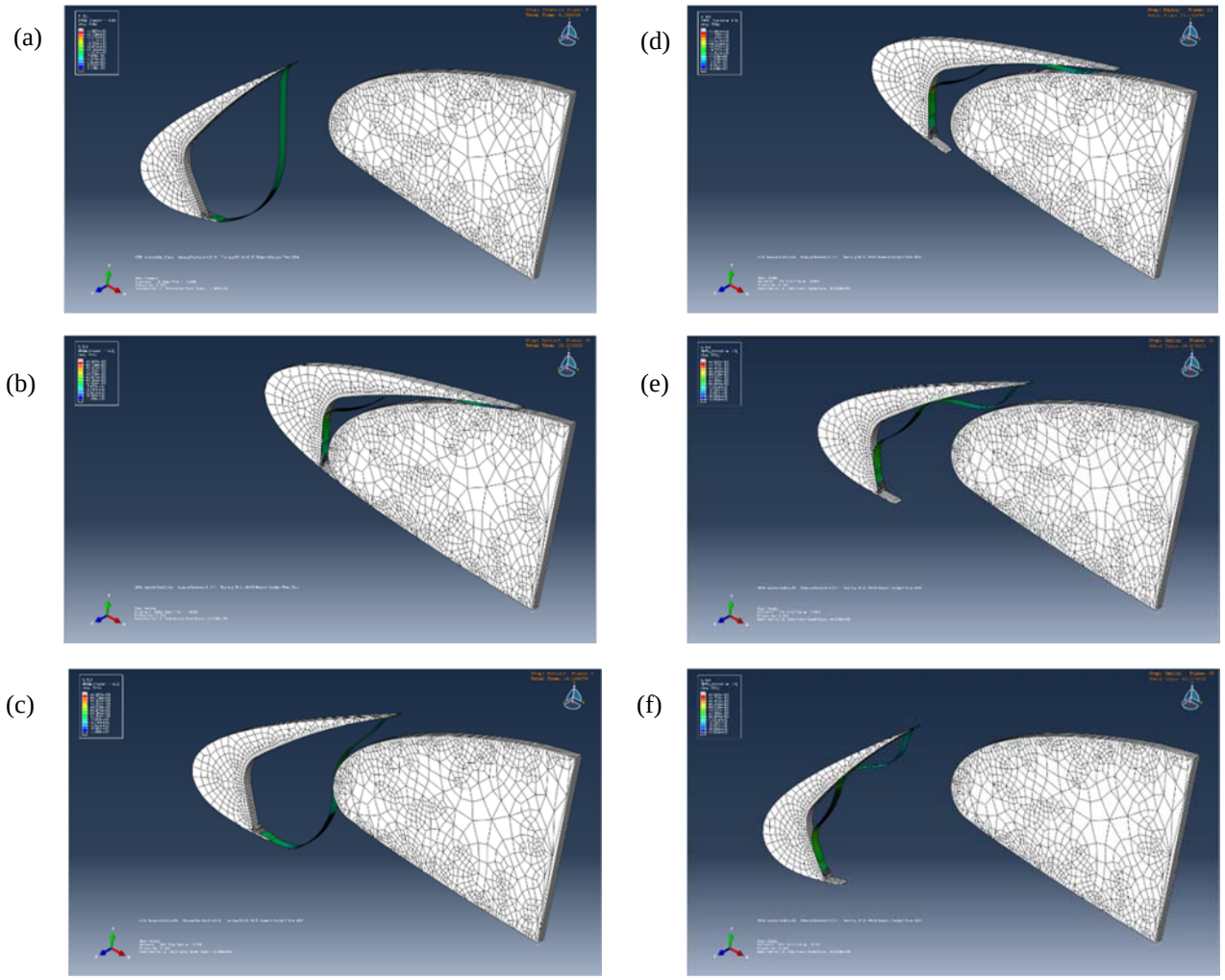

Figure 24. Computation modeling of SMP SCF actuation shows unsuccessful deployment with a mid-link (length: 4”, mean location from bottom: 4”). (a –c) retraction, and (d-f) deployment. A full animation is available at NTRS [23].

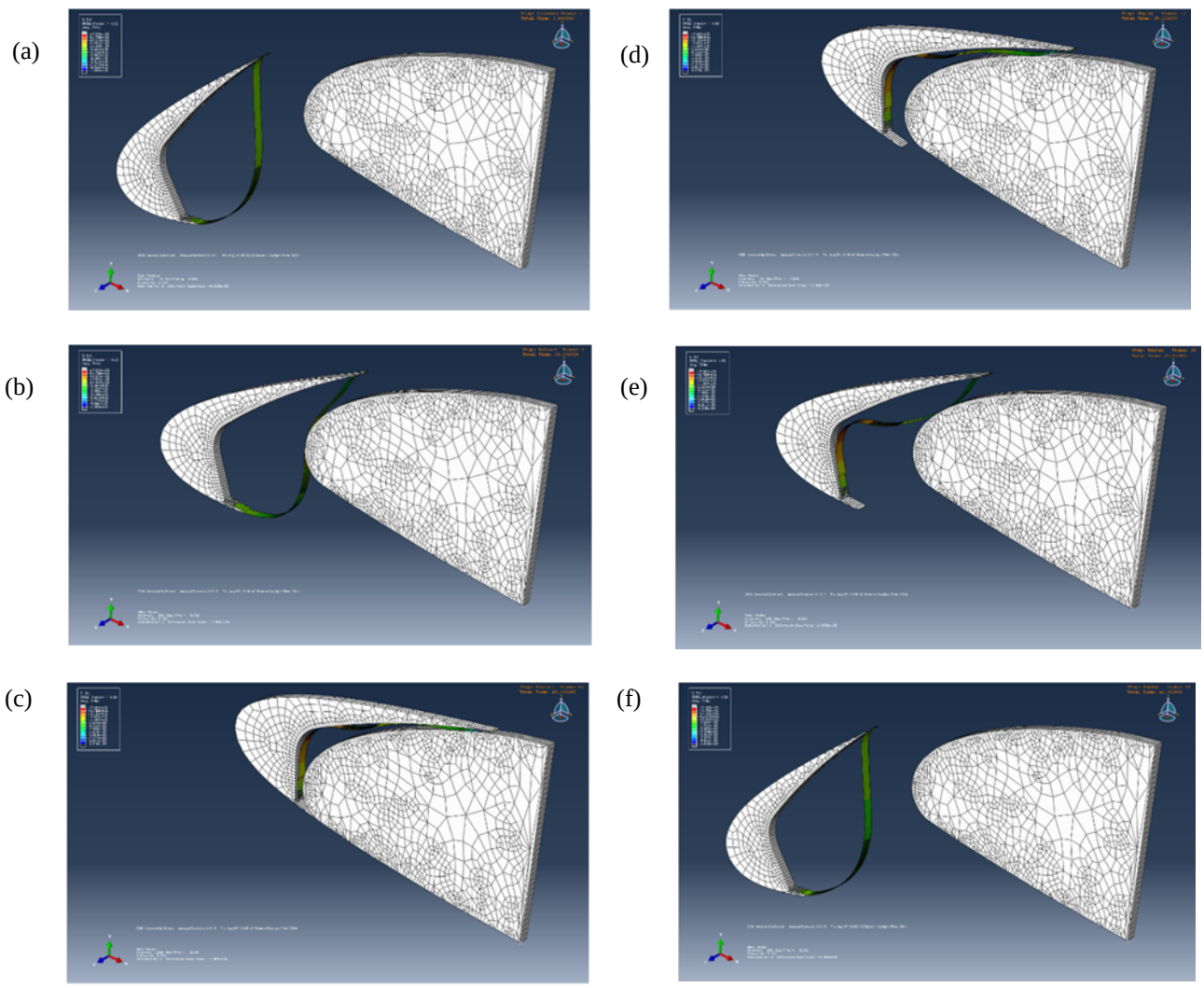

Figure 25. Computation modeling of SMP SCF actuation shows successful deployment with a mid-link (length: 3”, mean location from bottom: 6.5”). (a –c) retraction, and (d-f) deployment. A full animation is available at NTRS [24].

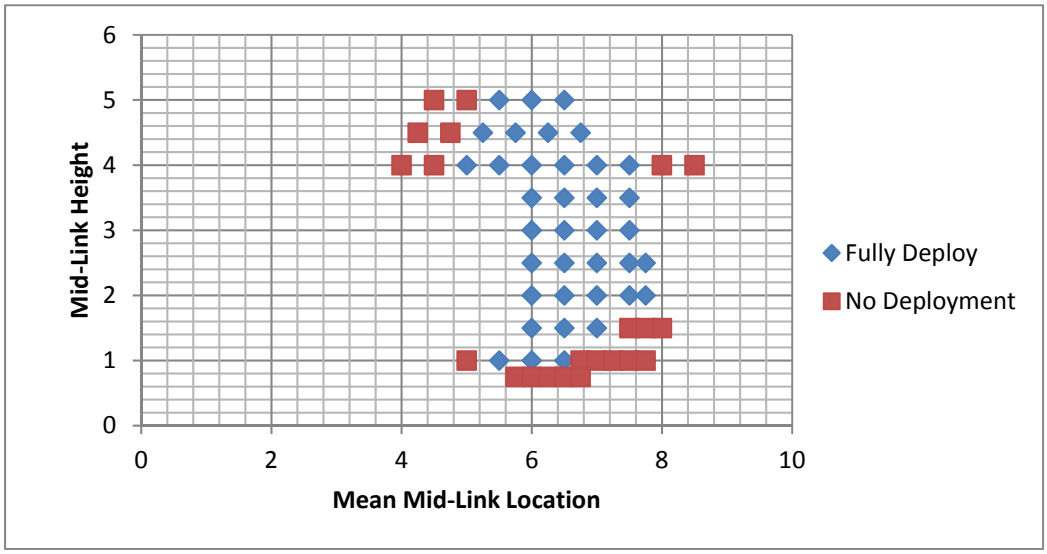

Figure 26. Optimization of mid-link height and location for successful deployment.

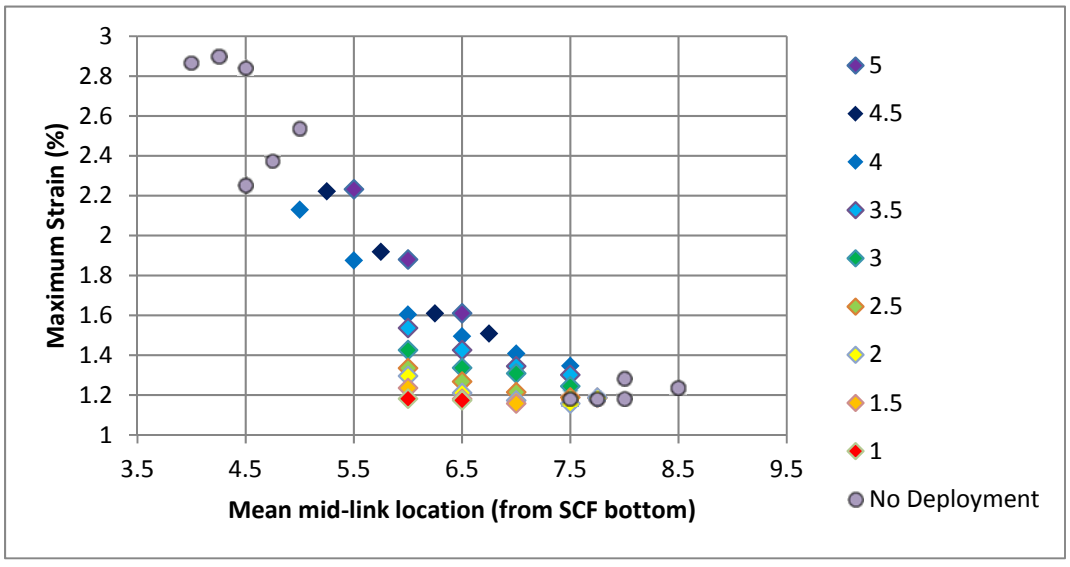

Figure 27. Maximum strain verses mid-link location for various mid-link sizes

3.3. Fabrication of Slat-Cove Filler (SCF) using SMP composite.

The slat-cove filler (SCF) for a bench-top demo was fabricated using the developed SMP composites. Figure 28 shows tooling and a fabricated SCF test specimen. Fiber reinforced SMP prepregs were stacked in the desired lay-ups in the tooling and cured in an autoclave. After curing, the sample was taken out, then cut and trimmed to get precise dimensions. The prepared SCF specimen was installed on the bench-top demo station to investigate its deployment and stowage performance as shown in Figure 29.

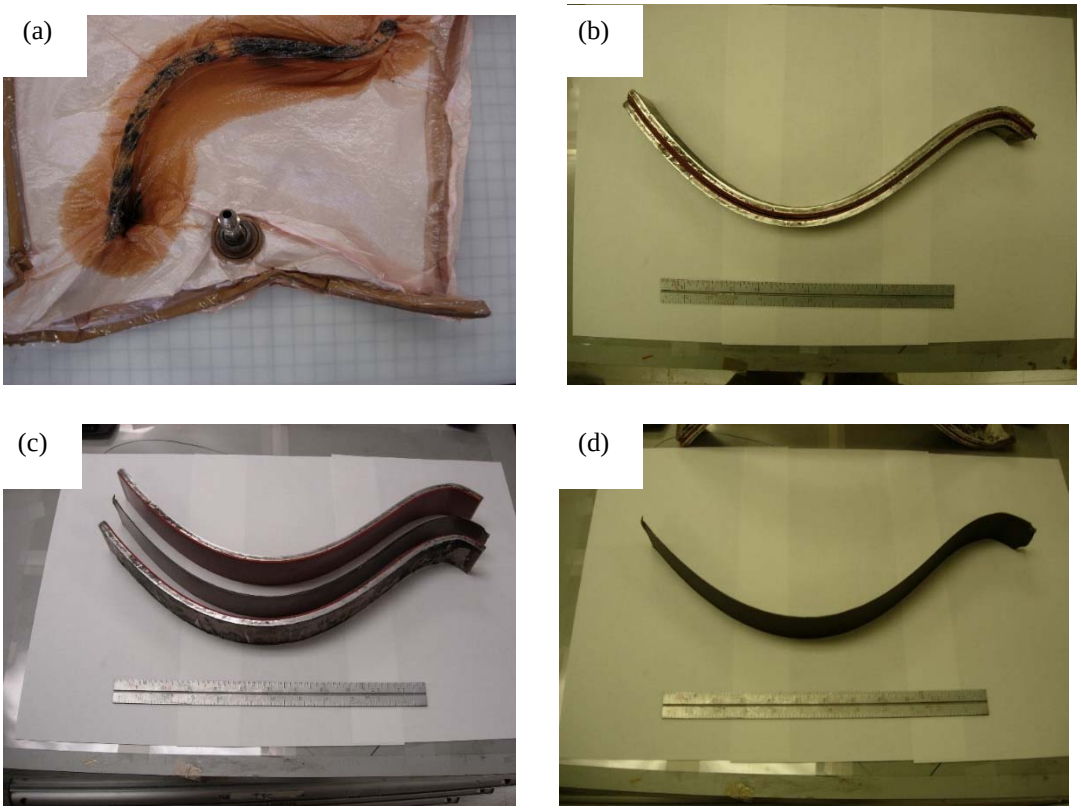

Figure 28. Fabrication of SCF using SMP composite. (a) sample mold in breathing fabric after curing in autoclave, (b) SMP SCF in aluminum mold, (c-d) retrieving SMP SCF sample from the aluminum mold.

3.5. Bench-top demonstration of SCF fabricated with various SMP composites.

The performance of a bench-top demonstration of slat-cove filler (SCF) fabricated with the developed various SMP composites was investigated.

3.5.1. SCF fabricated with LaRC shape memory polymer composite 1 (Carbonaceous nanophase doped SMP).

Figure 29 shows the performance of SCF fabricated with CNT doped SMP composite SCF. Glass to rubbery state transition was controlled by direct Joule heating. Top and bottom electrodes were predesigned according the Abaqus modeling (section 4) for optimum retraction/deployment performance. Mid-link section was not laminated by electrode so it maintained high stiffness during actuation. When the electric field was applied, top and bottom sections were heated to reduce the modulus for SCF retraction [Figure 29 (c)]. However, after deployment, a crack in the mid-link was found. This suggests that the strain at the mid-link was higher than the calculated value by Abaqus model.

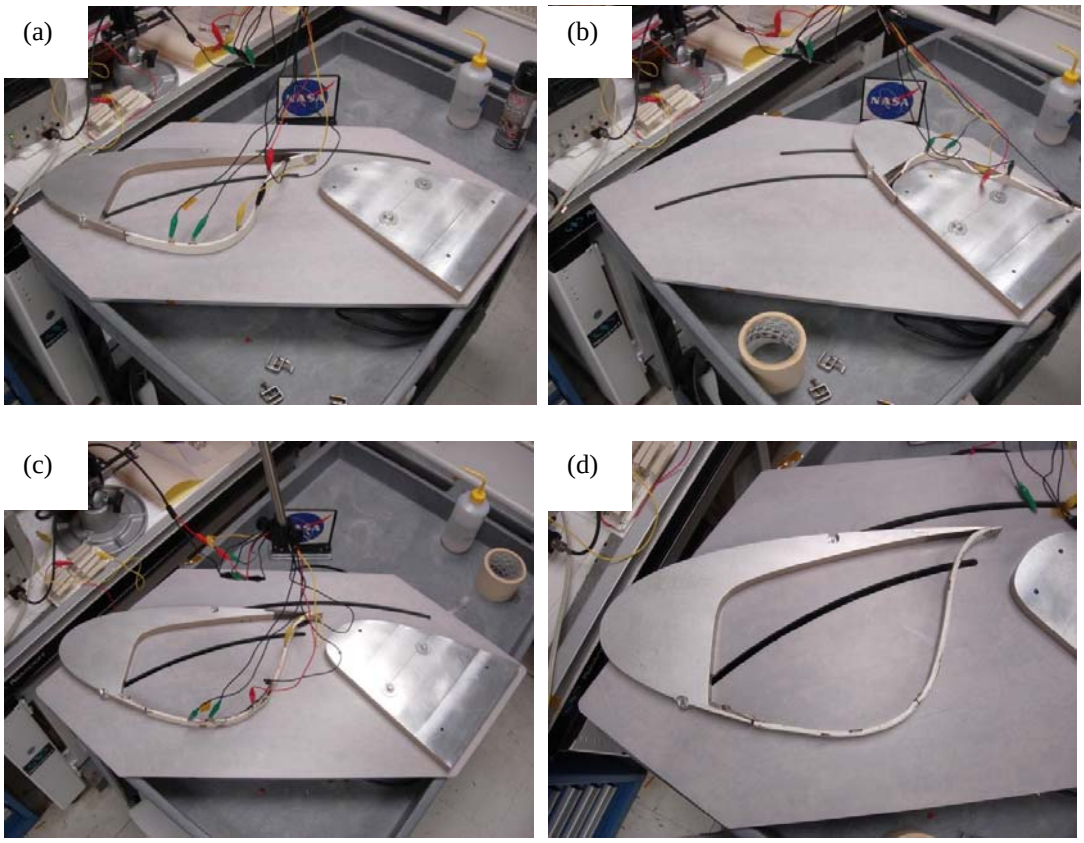

Figure 29. Bench-top demonstration of SCF fabricated with CNT doped SMP composite. (a) before retraction, (b) after retraction, (c) after deployment and (d) crack found in the mid-link after deployment.

3.5.2. SCF fabricated with LaRC shape memory polymer composite 2 (Kevlar® fiber fabric/SMP composite).

In order to improve the mechanical durability of SCF fabricated with SMP composite, the SCF was fabricated with Kevlar® fiber SMP composite (Kevlar® 29, 4HS, $[0°]_5$, Figure 30). Since the Kevlar® composite was not conductive enough for direct Joule heating, heating tape was applied to permit transition at the top and bottom sections [Figure 30 (b)]. A Nitinol spring was installed to enable smooth deployment. The SCF fabricated with Kevlar® fiber SMP composite showed successful deployment but during stowage, it kinked in the top and bottom sections [Figure 30 (c-h)]. A video of the full operation of SCF demo is available at NASA Technical Reports Server (NTRS) [28]. The kinks were permanent mechanical failures in the composite.

3.5.3. SCF fabricated with LaRC shape memory polymer composite 3 (Carbon fiber fabric/SMP composite).

Carbon fiber fabric was employed to solve the kink issue, because carbon fiber had better interfacial adhesion to the polymer matrix. The SCF was fabricated with carbon fiber (5HS, $[0°]_3$). It exhibited good deployment performance, but still kinked during stowage (Figure 31). However, even after multiple operation of stowage/deployment, no permanent damage was found at the location of the kinks. A video of the full operation of SCF demo is available at NASA Technical Reports Server (NTRS) [29]. Applying thin ply carbon fiber fabric composites did not help to solve the kink issues. However, when a thin shape memory alloy sheet (SMA, 0.5mm thick) was laminated to the thin ply carbon fabric comnposite, SCF sucessfully retracted and deployed without kinking. A video of the full operation the SMA laminated SCF is available at NASA Technical Reports Server (NTRS) [30].

3.5.4. SCF fabricated with LaRC shape memory polymer composite 4 (CNT sheet/SMP composite).

Another solution investigated was the insertion of carbon nanotube (CNT) sheets since CNT sheets were far more flexible than carbon fiber and had good interfacial adhesion to polymer

resins after appropriate modification. Figure 32 shows the full process of stowage and deployment. The SCF fabricated with CNT sheet/SMP composites were the first to yield successful stowage and deployment without kinks. However, the stowed elastic energy of CNT sheet/SMP composite was not as high as CF/SMP composites, resulting in sluggish performance. Lamination of thin shape memory alloy sheet (SMA, 0.25mm thick) improved the deployment performance. A video of the full operation of SCF demo is available at NASA Technical Reports Server (NTRS) [31].

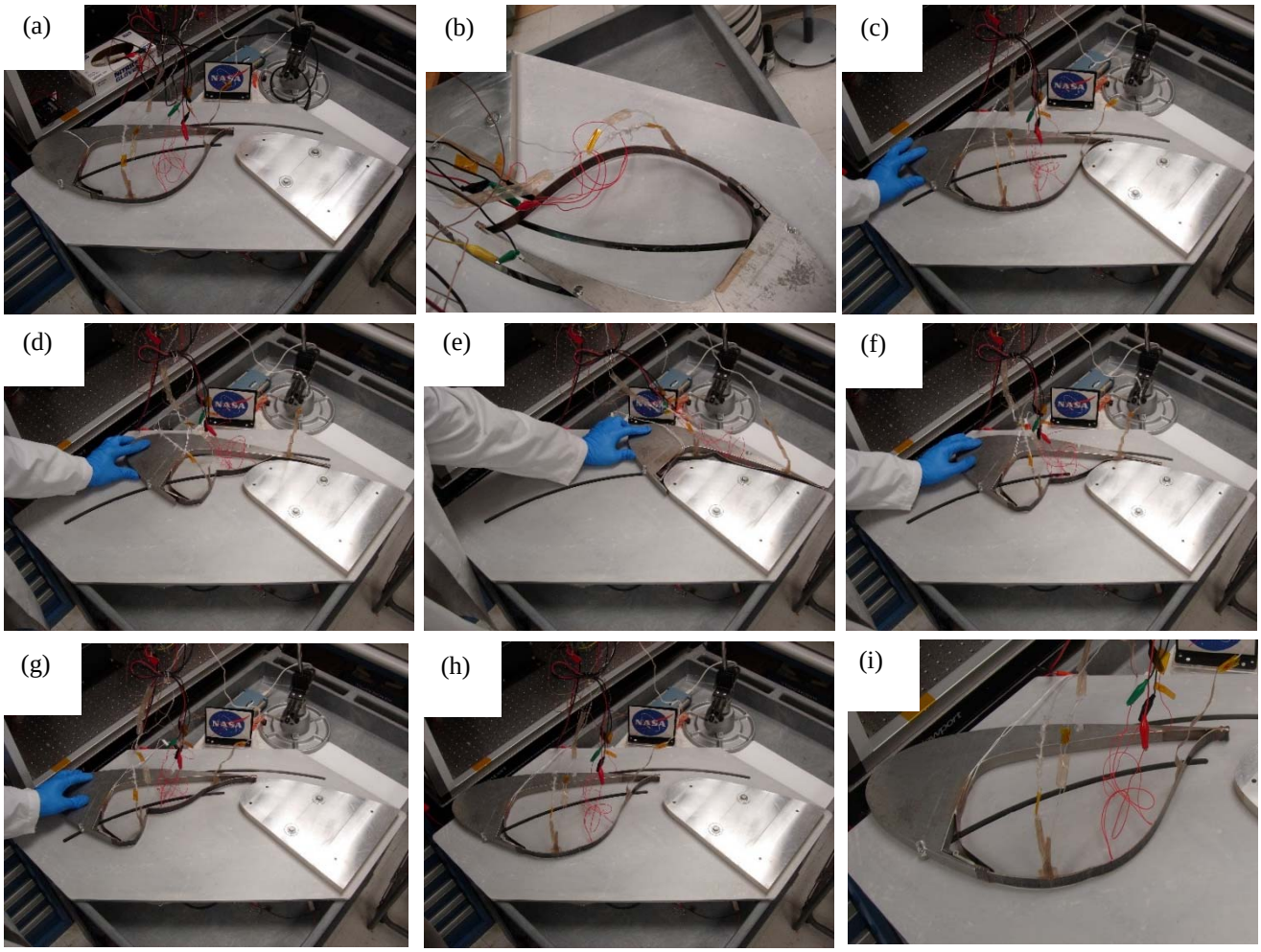

Figure 30. Bench-top demonstration of SCF fabricated with Kevlar® fiber/SMP composite. (a) before retraction, (b) heating tapes in top and bottom sections, Nitinol spring, (c-h) full process of stowage and deployment, and (i) showing a permanent damage after runs.

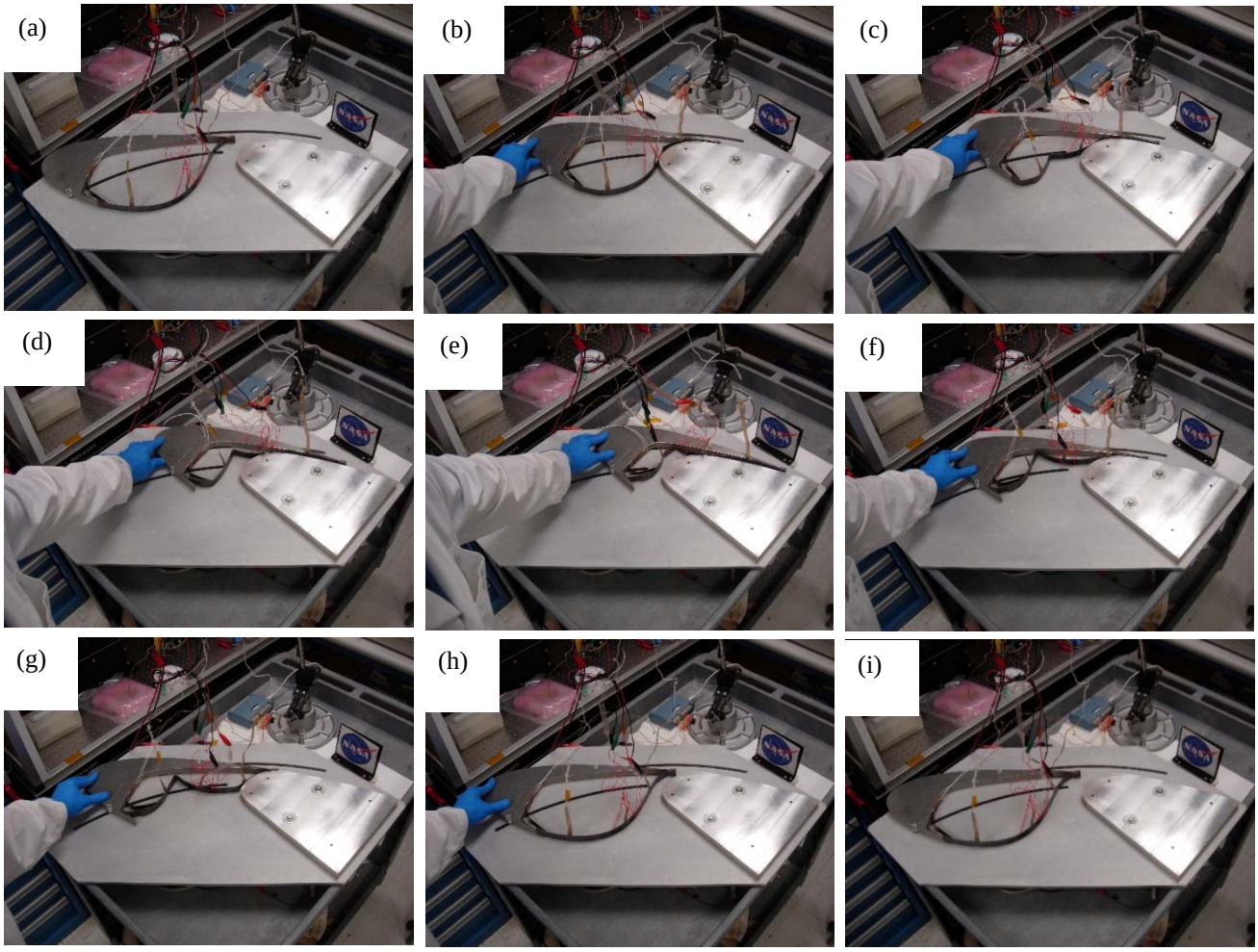

Figure 31. Bench-top demonstration of SCF fabricated with carbon fiber/SMP composite. (a) before retraction, (b-h) full process of stowage and deployment, and (i) showing no permanent damage after multiple runs.

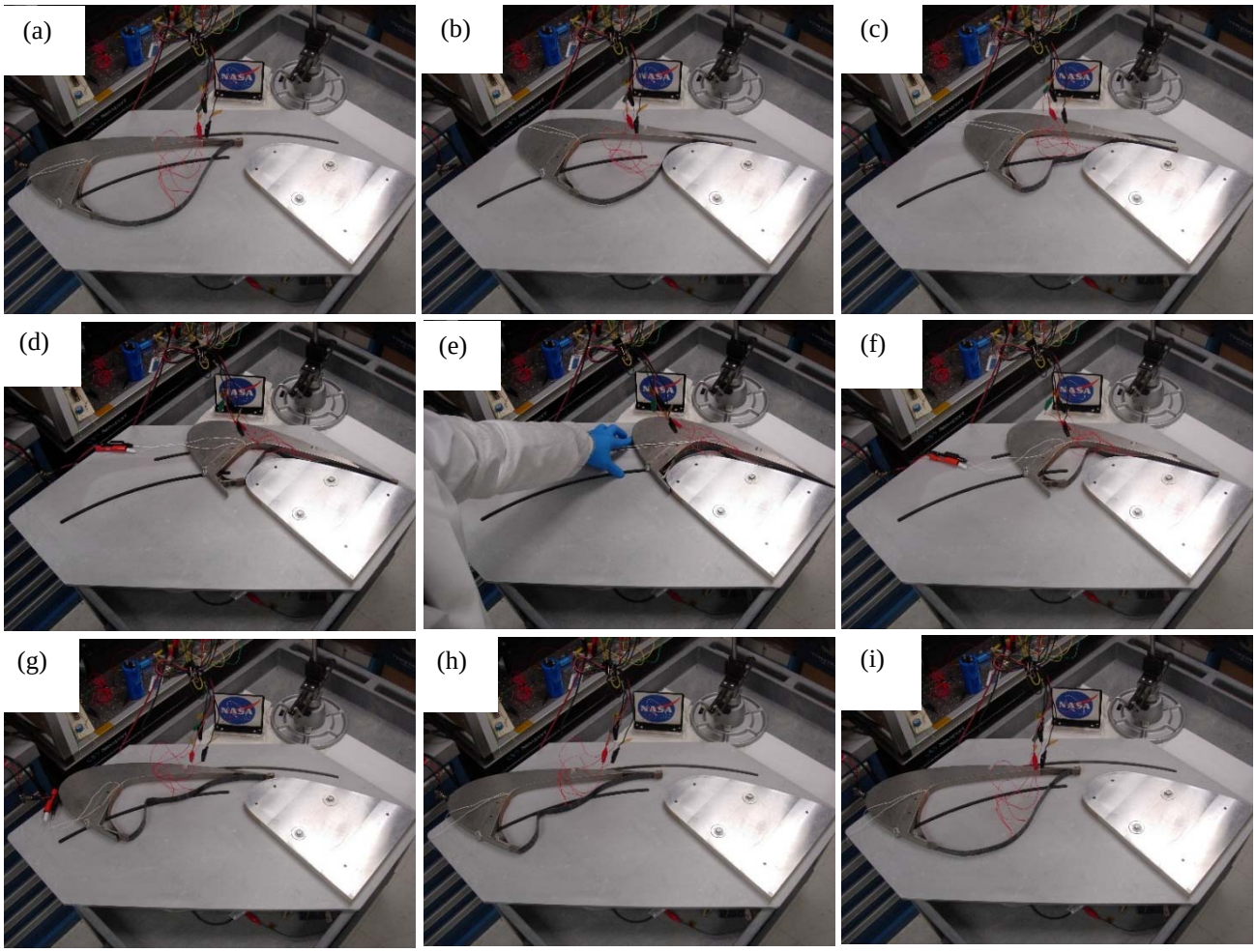

Figure 32. Bench-top demonstration of SCF fabricated with CNT sheet ($[0°]_{35}$)/SMP/SMA composite. (a) before retraction, (b-i) full process of stowage and deployment with no kink.

4. Conclusion

A new series of shape memory polymer composites (LaRC-SMPC) was developed for aircraft noise reduction application. Multilayered LaRC-SMPCs fabricated with elastic layers and different fibers [Kevlar®, carbon fiber (regular and thin ply), carbon nanotubes sheet] were characterized. The performance of slat-cove filler prototypes fabricated using various LaRC-SMPC compositions was investigated with a bench-top apparatus that was representative of modern transport-class airframe geometry. The SCFs made of Kevlar® fiber fabric or carbon fiber fabric infused SMPC kinked in simulated operation, which can be a critical mechanical problem for this application. The SCF made of CNT sheet/SMP composite can be autonomously deployed and stowed without kinking, but deployment was sluggish compared to the carbon fiber fabric/SMP composite. A balance of strain capability, redeployment speed and steady aero-load sustainment remained elusive in this study. Among the lessons learned in this materials development effort is the need to assess material properties in simulated use conditions. In this case, investigation of the SCF fabricated with LaRC-SMPC under simulated aerodynamic load exposed shortcomings in the material that would not have otherwise been noted.

Acknowledgement

Authors appreciate Messrs. Hoa Luong and Sean Britton for their effort on sample preparation and SC parameter optimization study.

References

[1] Scholten, W.; Patterson, R.; Hartl, D.; Strganac, T.; Volpi, J.; Chapelon, Q.; and Turner, T.: "Noise Reduction in a High Lift Wing Using SMAs: Computational Fluid-Structural Analysis," *Proc. ASME 2016 Conf. on Smart Matl., Adaptive Struct. and Intell. Sys.*, Stowe, VT, September 28-30, 2016.

[2] Choudhari, M. M.; and Khorami, M. R.: "Effect of Three-Dimensional Shear-Layer Structures on Slat-Cove Unsteadiness," *AIAA Journal*, Vol. 45, No. 9, 2007, pp. 2174-2186.

[3] Khorrami, M. D.; Berkman, M. E.; and Choudhari, M.: "Unsteady flow computations of a slat with a blunt trailing edge," *AIAA Journal*, Vol. 38, No. 11, 2000, pp. 2050-2058.

[4] Singer, B. A.; Lockard, D. P.; and Brentner, K. S.: "Computational Aeroacoustic Analysis of Slat Trailing-Edge Flow," *AIAA Journal*, Vol. 38, No. 9, 2000, pp. 1558-1564.

[5] Khorrami, M. R.; Singer, B. A.; and Berkman, M. E.: "Time-accurate Simulations and Acoustic Analysis of Slat Free Shear Layer," *AIAA Journal*, Vol. 40, No. 7, 2002, pp. 1284-1291.

[6] Khorrami, M. R.; Singer, B. A.; and Lockard, D. P.: "Time-accurate Simulations and Acoustic Analysis of Slat Free Shear Layer: Part II," *8th AIAA/CEAS Aeroacoustics Conf. & Exhibit*, Breckenridge, CO, June 17-19, 2002.

[7] Streett, C. L.; Casper, J. H.; Lockard, D. P.; Khorrami, M. R.; Stoker, R. W.; Elkoby, R.; Wenneman, W. F.; and Underbrink, J. R.: "Aerodynamic Noise Reduction for High-Lift Devices on a Swept Wing Model," *44th AIAA Aerospace Sci. Meeting & Exhibit, Reno, NV*, January 9-12, 2006.

[8] Imamura, T.; Ura, H.; Yokokawa, Y.; Enomoto, S.; Yamamoto, K.; and Hirai, T.: "Designing of Slat-Cove Filler as a Noise Reduction Device for Leading-edge Slat," *13th AIAA/CEAS Aeroacoustics Conf.*, Rome, Italy, May 21-23, 2007

[9] Turner, T. L.; Kidd, R. T.; Hartl, D. J.; and Scholten, W. D.: "Development of a SMA-Based, Slat-Cove Filler for Reduction of Aeroacoustic Noise Associated with Transport-Class Aircraft Wings," *Proc. ASME 2013 Conf. on Smart Matl., Adaptive Struct. and Intell. Sys.*, Snowbird, UT, September 16-18, 2013.

[10] Scholten, W. D.; Hartl, D. J.; and Turner, T. L.: "Analysis-Driven Design Optimization of a SMA-Based Slat-Cove Filler for Aeroacoustic Noise Reduction," *Proc. ASME 2013 Conf. on*

Smart Matl., Adaptive Struct. and Intell. Sys., SMASIS2013-3104, Snowbird, UT, September 16-18, 2013.

[11] Scholten, W. D.; Hartl, D. J.; Turner, T. L.; and Kidd, R. T.: "Development and Analysis-Driven Optimization of a Superelastic Slat-Cove Filler for Airframe Noise Reduction," *AIAA Journal*, Vol. 54, No. 3, 2016, pp. 1074-1090.

[12] Rainer, W.C; Redding, E. M.: "Irradiated, Cross-linked Polyethylene Copolymer," US patent 2,234,993.

[13] Lendlein, A; Langer, R. S.: "Biodegradable Shape Memory Polymeric Sutures," US patent 8,303,625.

[14] Otsuka, K.; Wayman, C. M. eds.: "Shape Memory Polymers," Cambridge University Press, Cambridge, 1998.

[15] Tobushi, H.; Hara, H.; Yamada, E.; Hayashi, S.: "Thermomechanical Properties in a Thin Film of Shape Memory Polymer of Polyurethane Series," *Smart Mater. Struct.* Vol. 5, 1996, pp. 483 - 491.

[16] Xu, J.; Shi, W.; and Pang, W.: "Synthesis and Shape Memory Effects of Si-O-Si cross-linked hybrid polyurethane," *Polymer* Vol. 47, 2006, pp. 457-465.

[17] Jing, X.; Liu, Y.; Liu, Y.; and Tan, H.: "Preparation and Properties of Shape Memory Epoxy Resin Composites," *Appl. Mech. Mater.* Vol. 214, 2012, pp. 12-16.

[18] Tong, T. H.; Vining, B.; Hreha, R.; and Barneli, T.; "Shape Memory Epoxy Copolymers," US patent application 20080269420.

[19] Ohki,T.; Ni, Q. –Q.; Ohsako, N.; and Iwamoto, M.: "Mechanical and Shape Memory Behavior of Composites with Shape Memory Polymer," *Composites A*, Vol. 35, 2004, pp. 1065-1073.

[20] Liu, Y.; Gall, K.; Dunn, M. L.; and McCluskey, P.: "Thermomechanics of Shape Memory Polymer Nanocomposites," *Mech. Mater.*, Vol. 36, 2006, pp. 929-940.

[21] Koerner, H.; Price, G.; Pearce, N. A.; Alexander, M.; and Richard, A. V.: "Remotely Actuated Polymer Nanocomposites – Stress-Recovery of Carbon-Nanotube-Filled Thermoplastic Elastomer," *Nat. Mater.* Vol. 3, 2004, pp. 115-120.

[22] Cho, J. H.; Kim, J. W.; Jung, Y. C.; and Goo, N. S.; "Electroactive Shape-Memory Polyurethane Composites Incorporating Carbon Nanotubes," *Macromol. Rapid Commun.* Vol. 26, 2005, pp. 412-416.

[23] Schmid, A. M: "Electromagnetic Activation of Shape Memory Polymer Networks Containing Magnetic Nanoparticles," *Macromol. Rapid Commun.* Vol. 27, 2006, pp. 1168-1172.

[24] Video clip, "Shape memory effect demo.mp4" is availble in the additional supporting information. Shows the visual demonstration of shape memory effect of developed LaRC-SMP (white colored specimen) and LaRC-SMPC (black colored specimen). The program-shaped specimens (U shape) transformed to their original shape (straight shape) in an environment oven at 120°C.

[25] Video clip, "Modeling-No mid link.mp4" is availble in the addtional supporting information.

[26] Video clip, "Modeling-Mid link-No Deploy.mp4" is availble in the additional supporting information.

[27] Video clip, "Modeling-Mid link-Deploy.mp4" is availble in the additional supporting information.

[28] Video clip, "Kevlar-SMP-SCF-Demo.mp4" is availble in the additional supporting information.

[29] Video clip, "CF-SMP-SCF-Demo.mp4" is availble in the additional supporting information.

[30] Video clip, "Thin CF-SMP-SMA-SCF-Com-Demo.mp4" is availble in the additional supporting information.

[31] Video clip, "CNT sheet-SMP-SMA-SCF-Demo.mp4" is availble in the additional supporting information.

APPENDIX

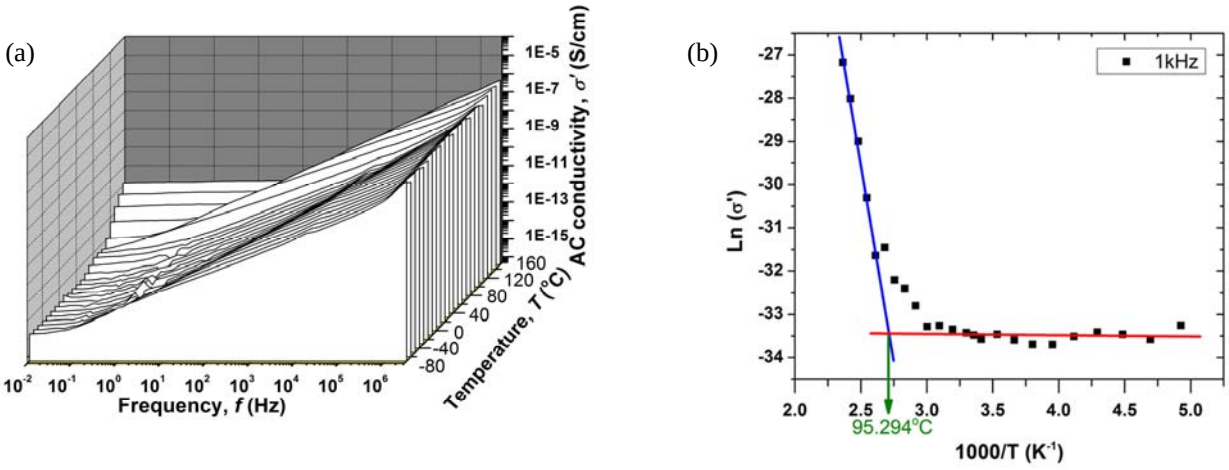

Figure S1. (a) AC conductivity of LaRC-SMP as function of temperature and frequency, and (b) logarithm of AC conductivity as a function of inversed temperature.

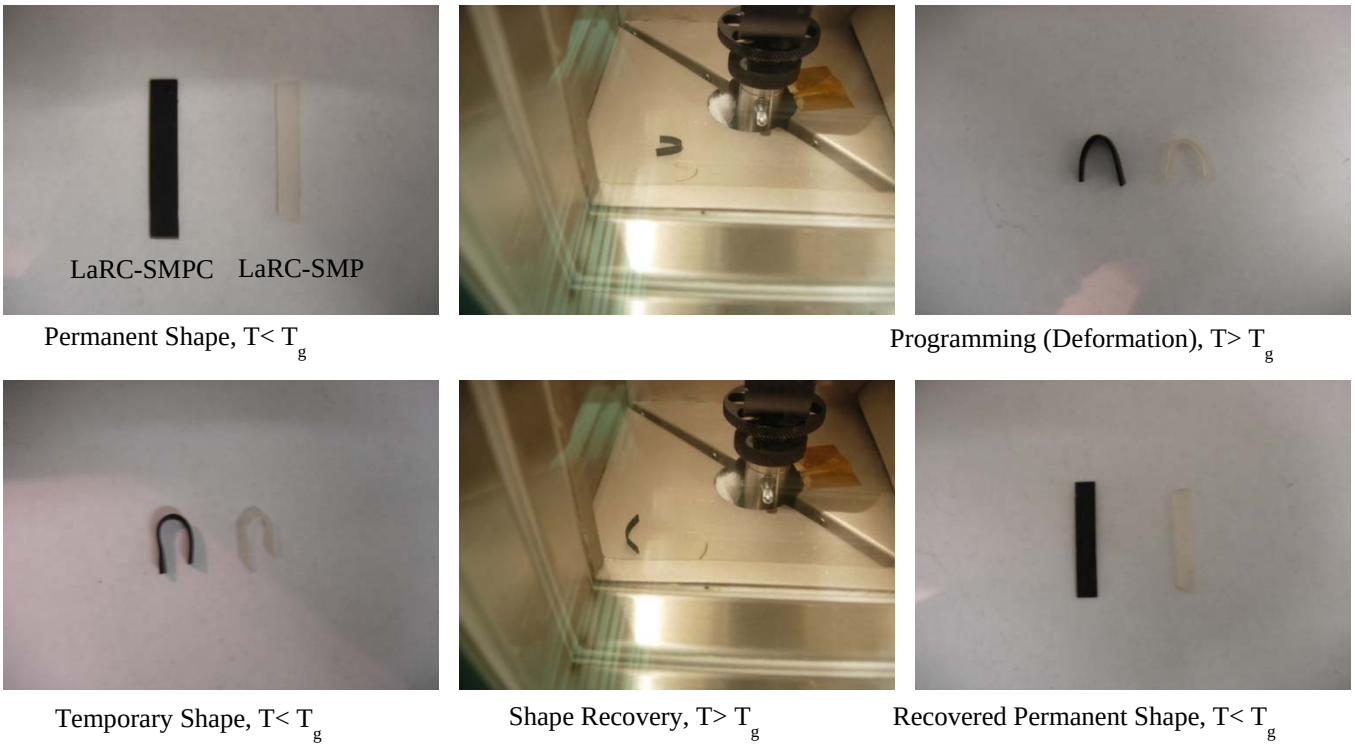

Figure S2. Shape memory effect of LaRC-SMP and LaRC-SMPC.

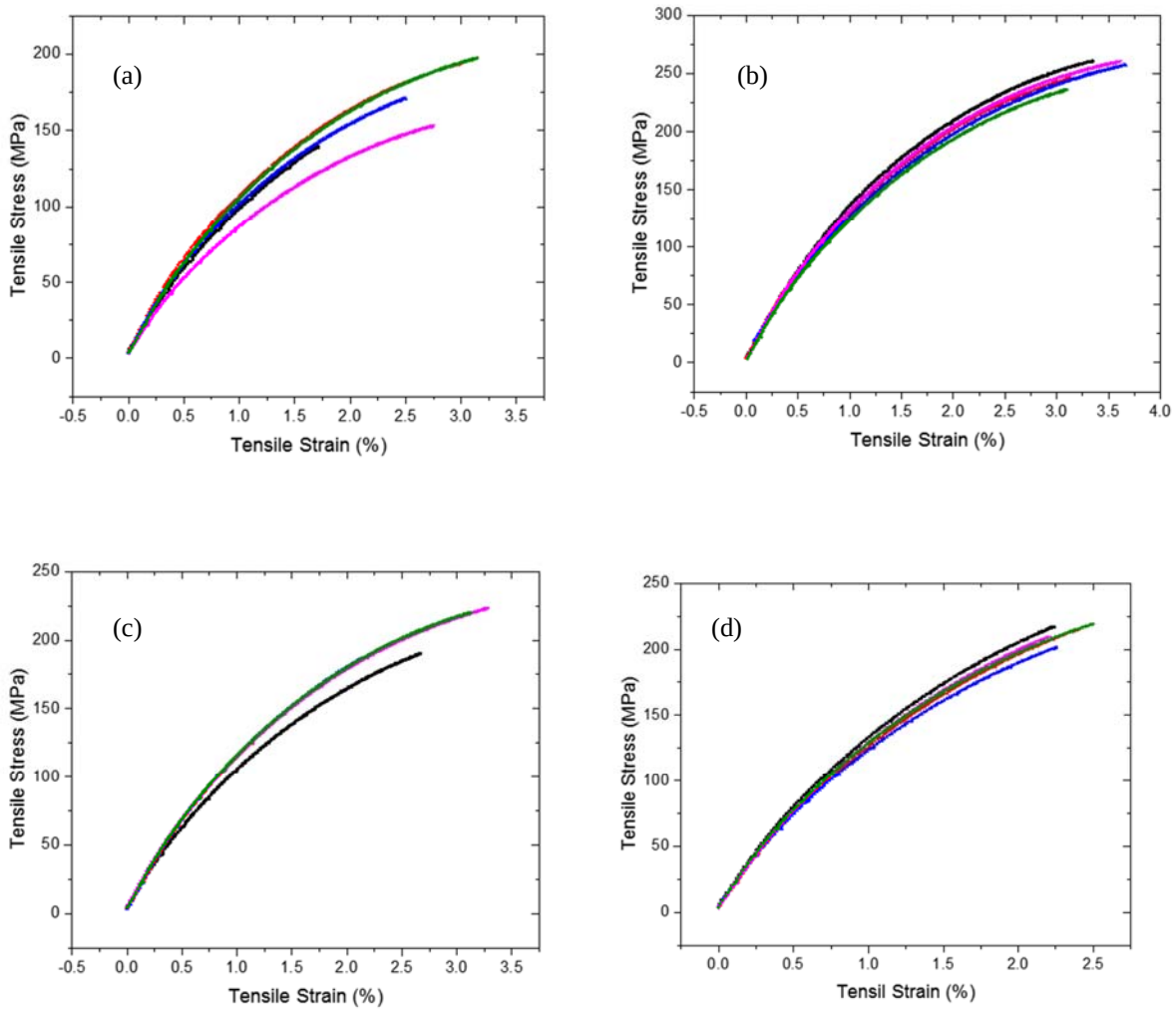

Figure S3. Tensile properties of (a) pristine CNT/LaRC-SMP, (b) thermal treated CNT/LaRC-SMP, (c) sized CNT/LaRC-SMP, and (d) thermal & sized CNT/SMP.

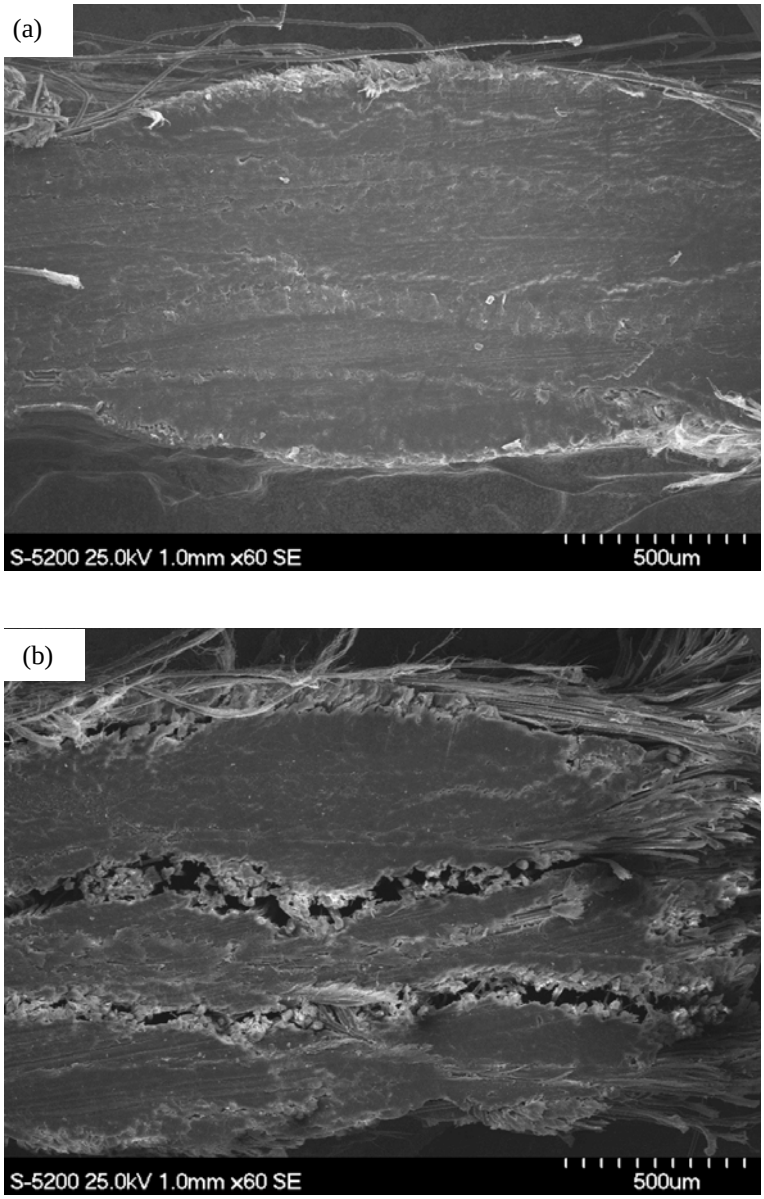

Figure S4. Cross-sectional morphology of Kevlar fiber doped SMPC. (a) before bending actuation and (b) after bending actuation.

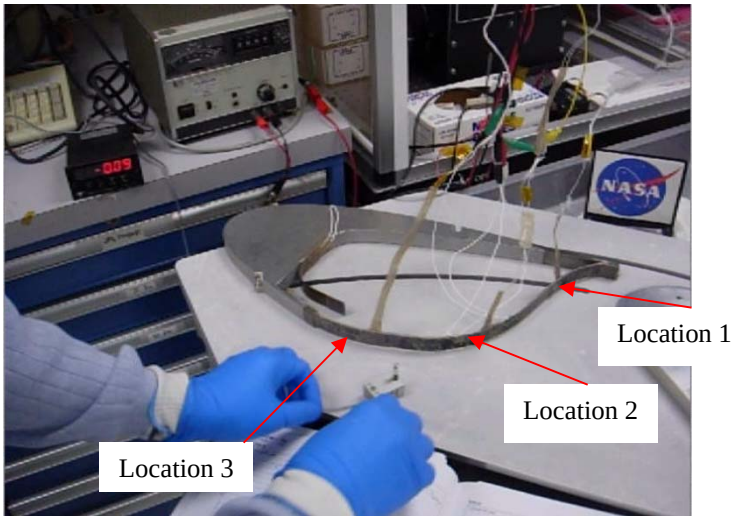

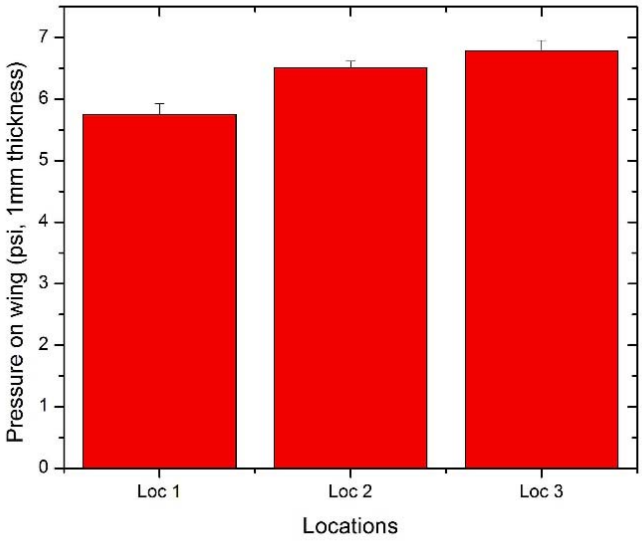

Figure S5. Actuation load requiring for the retraction of SMP SCF.

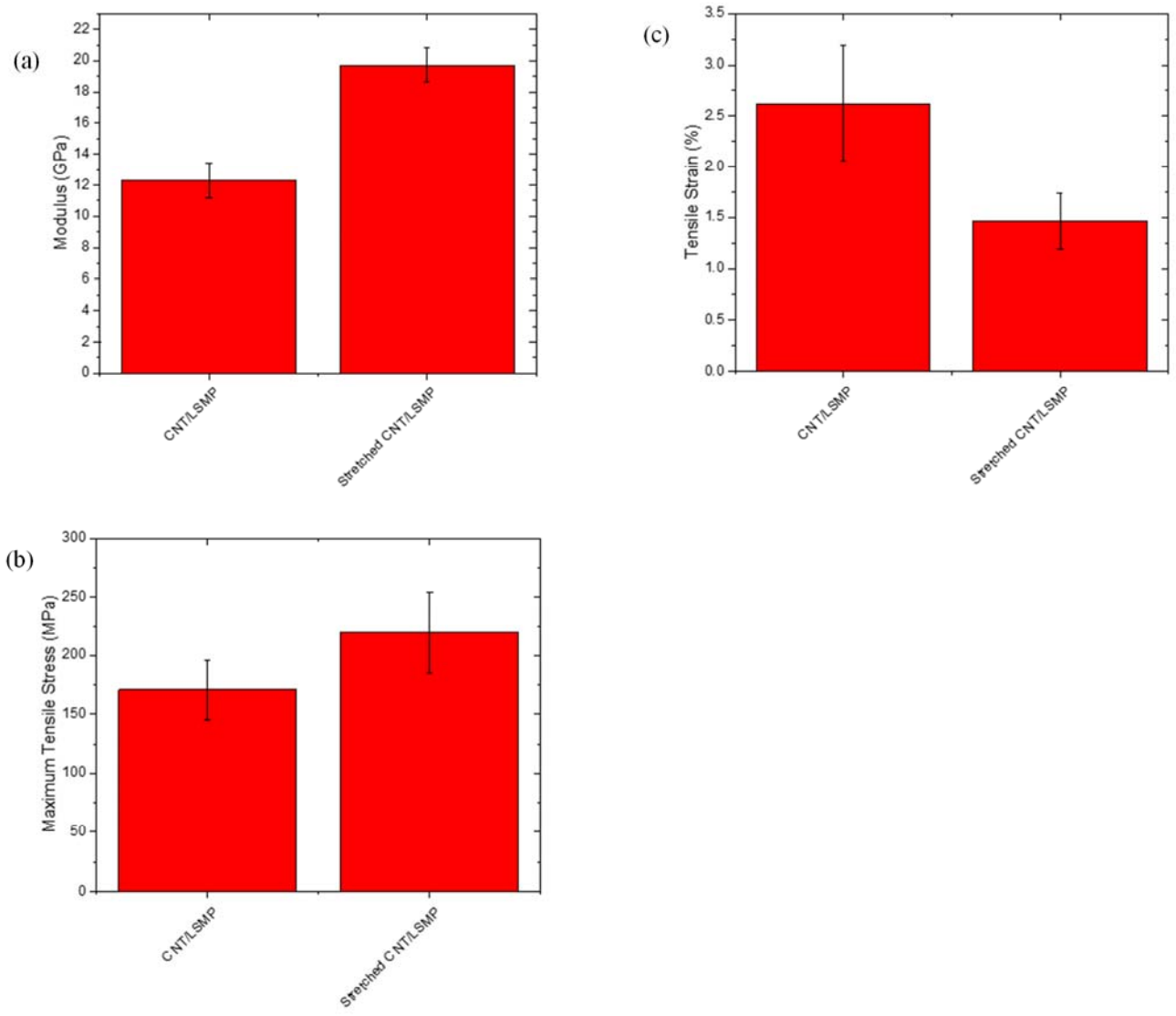

Figure S6. Tensile properties of CNT sheet/LaRC-SMP and stretched CNT sheet (40%)/LaRC-SMP. (a) modulus, (b) maximum tensile stress and (c) strain at break.

Additional Supporting Information

Additional multimedia information is available at “Supplemental Video files DOC ID# 20180000970 in STI Program multimedia repository”. List of the video supporting information is:

(1) “Shape memory effect demo.mp4” (for Reference 21, Fig. 13 & Fig. S2) – Shows the visual demonstration of shape memory effect of developed LaRC-SMP (white colored specimen) and LaRC-SMPC (black colored specimen). The program-shaped specimens (U shape) transformed to their original shape (straight shape) in an environment oven at 120°C.
(2) “Modeling-No mid link.mp4” (for Reference 22, Fig. 23) – shows the animation of modeling of SCF parameter optimization.
(3) “Modeling-Mid link-No Deploy.mp4” (for Reference 23, Fig. 24) – shows the animation of modeling of SCF parameter optimization.
(4) “Modeling-Mid link-Deploy.mp4” (for Reference 24, Fig. 25) – shows the animation of modeling of SCF parameter optimization.
(5) “Kevlar-SMP-SCF-Demo.mp4” (for Reference 25, Fig. 30) – shows the full operation of a bench-top model of Kelvar® fiber fabric/SMP composite based SCF.
(6) “CF-SMP-SCF-Demo.mp4” (for Reference 26, Fig. 31) – shows the full operation of a bench-top model of CF fabric/SMP composite based SCF.
(7) “Thin CF-SMP-SMA-SCF-Com-Demo.mp4” (for Reference 27) – shows the full operation of a bench-top model of thin CF fabric/SMP composite/SMA lamination based SCF.
(8) “CNT sheet-SMP-SMA-SCF-Demo.mp4” (for Reference 28, Fig. 32)– shows the full operation of a bench-top model of CNT sheet/SMP composite/SMA laminated based SCF.

REPORT DOCUMENTATION PAGE

Form Approved
OMB No. 0704-0188

1. REPORT DATE *(DD-MM-YYYY)*
1-07-2018

2. REPORT TYPE
Technical Memorandum

3. DATES COVERED *(From - To)*

4. TITLE AND SUBTITLE
A Study of Shape Memory Polymer Based Slat-Cove Filler

5a. CONTRACT NUMBER

5b. GRANT NUMBER

5c. PROGRAM ELEMENT NUMBER

6. AUTHOR(S)
Kang, Jin Ho; Siochi, Emilie J.; Turner, Travis L.; Penner, Ronald K.; Thomas, Richard; Sean Brown

5d. PROJECT NUMBER

5e. TASK NUMBER

5f. WORK UNIT NUMBER
561581.02.08.07

7. PERFORMING ORGANIZATION NAME(S) AND ADDRESS(ES)
NASA Langley Research Center
Hampton, VA 23681-2199

8. PERFORMING ORGANIZATION REPORT NUMBER
L-20948

9. SPONSORING/MONITORING AGENCY NAME(S) AND ADDRESS(ES)
National Aeronautics and Space Administration
Washington, DC 20546-0001

10. SPONSOR/MONITOR'S ACRONYM(S)
NASA

11. SPONSOR/MONITOR'S REPORT NUMBER(S)
NASA-TM-2018-219804

12. DISTRIBUTION/AVAILABILITY STATEMENT
Unclassified
Subject Category 24
Availability: NASA STI Program (757) 864-9658

13. SUPPLEMENTARY NOTES
Supplemental Video files in STI multimedia repository, DOC ID# 20180000970.

14. ABSTRACT
Aircraft noise reduction is an application of current intense interest for which smart materials show significant potential. Specifically, the aeroacoustic noise produced by the unsteady aerodynamic flow about the leading-edge high-lift device, such as leading-edge slat, of typical transport-aircraft wings is of particular interest. Concepts with the most promise to mitigate this noise source, most notably the slat-cove filler concept, have focused on highly reconfigurable structures that change shape between different phases of the flight envelope. These shape changes often involve large deformation, which has stimulated the consideration of shape memory materials. In recent years, shape memory materials (SMMs) have drawn greater interest for applications such as smart fabrics, intelligent medical devices, self-deployable space structures, morphing structures and packaging. Compared to other shape memory materials, like shape memory alloys (SMAs) or shape memory ceramics (SMCs), shape memory polymers (SMPs) have desirable advantages such as high elastic deformation to enable large shape change, broad tailorability of mechanical properties, potential biocompatibility and biodegradability, ductility, light weight and ease of processing.

15. SUBJECT TERMS
Airframe noise; Composite; Shape Memory Polymer; Slat-cove filler

16. SECURITY CLASSIFICATION OF:			17. LIMITATION OF ABSTRACT	18. NUMBER OF PAGES	19a. NAME OF RESPONSIBLE PERSON
a. REPORT	b. ABSTRACT	c. THIS PAGE			STI Help Desk (email: help@sti.nasa.gov)
U	U	U	UU	53	19b. TELEPHONE NUMBER *(Include area code)* (757) 864-9658